Dept. of Math. University of Oslo
Pure Mathematics
ISBN 82–553–1385–0 No. 19
ISSN 0806–2439 June 2003

ON A DIFFUSIVELY CORRECTED KINEMATIC-WAVE TRAFFIC MODEL WITH CHANGING ROAD SURFACE CONDITIONS

R. BÜRGER[A] AND K.H. KARLSEN[B]

Abstract. The well-known Lighthill-Whitham-Richards kinematic traffic flow model for unidirectional flow on a single-lane highway is extended to include both abruptly changing road surface conditions and drivers' reaction time and anticipation length. The result is a strongly degenerate convection-diffusion equation, where the diffusion term, accounting for the drivers' behaviour, is effective only where the local car density exceeds a critical value, and the convective flux function depends discontinuously on the location. It is shown that the validity of the proposed traffic model is supported by a recent mathematical well-posedness (existence and uniqueness) theory for quasilinear degenerate parabolic convection-diffusion equations with discontinuous coefficients [18, 20]. This theory includes a convergence proof for a monotone finite-difference scheme, which is used herein to simulate the traffic flow model for a variety of situations.

1. Introduction

The classical Lighthill-Whitham-Richards (LWR) kinematic wave traffic flow model [23, 24, 29] for unidirectional flow on a single-lane highway starts from the following "principle of conservation of cars":

$$\partial_t \rho(x,t) + \partial_x\big(\rho(x,t)v(x,t)\big) = 0, \tag{1.1}$$

where ρ is the density of cars as a function of distance x and time t and $v(x,t)$ is the velocity of the car located at point x at time t. The decisive constitutive assumption is that v is a function of the density ρ only, which results in the scalar conservation law

$$\partial_t \rho + \partial_x\big(\rho v(\rho)\big) = 0, \quad x \in \mathbb{R},\, t > 0, \tag{1.2}$$

where $v(\rho)$ is the car velocity at density ρ. In other words, we assume that each car's driver instantaneously adjusts his velocity to the local car density. There exists a variety of functions $v(\rho)$ suggested in the literature, see [15, 25] and the discussion in Section 2.1. We consider here the common choice

$$v(\rho) = v_{\max} V(\rho), \tag{1.3}$$

where $v_{\max}$ is a maximum velocity a driver would assume on a free highway, and $V(\rho)$ is a 'hindrance' function taking into account the presence of other cars that urge each driver to reduce his speed. Thus, $\rho v(\rho) = v_{\max} f(\rho)$, where we define

$$f(\rho) := \begin{cases} \rho V(\rho) & \text{for } 0 \le \rho \le \rho_{\max}, \\ 0 & \text{for } \rho < 0 \text{ and } \rho > \rho_{\max}, \end{cases} \tag{1.4}$$

Date: June 2, 2003.
Key words and phrases. Traffic flow model, conservation laws, convection-diffusion equations, discontinuous numerical flux, finite difference scheme, numerical simulation.
AMS subject classification. 35K65, 35L65, 90B20.

[A]Institute of Applied Analysis and Numerical Simulation, University of Stuttgart, Pfaffenwaldring 57, D-70569 Stuttgart, Germany. E-Mail: buerger@mathematik.uni-stuttgart.de.

[B]Department of Mathematics, University of Bergen, Johs. Brunsgt. 12, N-5008 Bergen, Norway, and Centre of Mathematics for Applications (CMA), Department of Mathematics, University of Oslo, P.O. Box 1053, Blindern, N–0316 Oslo, Norway. E-Mail: kennethk@mi.uib.no.

where $\rho_{\max}$ is the maximum car density corresponding to the 'bumper-to-bumper' situation. The simplest choice is the linear interpolation

$$V(\rho) = V_{\mathrm{LI}}(\rho) = 1 - \rho/\rho_{\max}. \tag{1.5}$$

Over the years, numerous extensions and improvements of the LWR model have been proposed. In this paper, we consider an extension by Mochon [26] of the LWR model to roads with (abruptly) changing surface conditions, which gives rise to a new flux density function $f(x,\rho)$ that varies discontinuously with respect to x, and combine it with the diffusively corrected kinematic wave model (DCKWM) analyzed by Nelson [27, 28], which leads to an additional second-order diffusion term on the right-hand side of (1.2). This diffusion term accounts for the drivers' anticipation length and reaction time. The result is a strongly degenerate parabolic convection-diffusion equation, where the flux density function and possibly the diffusion term depend on parameters which are discontinuous functions of the location x. Related models associating drivers' behaviour with a nonlinear diffusion term are discussed in [3, 32]. A general discussion of recent developments in traffic flow modeling is given in [2]. On the other hand, similar equations with discontinuous flux *and* degenerate diffusion appear in mathematical models of continuous sedimentation in ideal clarifier-thickener units [5]. It is the purpose of this paper to demonstrate that a new existence and uniqueness theory for these equations [18, 20], including a convergence proof for a finite difference scheme, can be applied to the traffic model sketched above, which, of course, includes the LWR model, Mochon's analysis [26], and the DCKWM model as special cases.

We are well aware that scalar continuum models for traffic flow present a strong simplification, and that more sophisticated "second-order" models (see e.g. [1, 9, 14, 17, 21]), including both scalar second-order partial differential equations and first-order systems of two equations (one 'continuity' and one 'linear momentum' equation), have caused quite some controversy in the traffic flow community. However, only recent results have made it possible to embed the model outlined here into a well-posedness theory. Having said this, we mention that Li [22] recently analyzed a hyperbolic first-order system of two conservation laws with relaxation and source terms, which can also be regarded as a second-order extension of the LWR model and has ingredients very similar to the model studied herein; namely, an x-(location-)dependent variation of the maximal velocity $v_{\max}$, and a relaxation time. Li's well-posedness analysis [22] is essentially based on the assumption that $v_{\max}$ is a *smooth* function of x. Thus, our paper shows (although for a simpler model) that such a smoothness assumption is not a necessary requirement in order to establish well-posedness for a continuum traffic flow model.

This paper is organized as follows. In Section 2 the extensions of the LWR model to abruptly changing road surface conditions and to the DKWM model by Mochon [26] and Nelson [27, 28] are recalled and combined into a the new diffusively corrected kinematic-wave model with changing road surface conditions. In Section 3 the new mathematical theory of degenerate parabolic equations with discontinuous coefficients [18, 20] is applied to the present problem. The results are an appropriate entropy solution concept defining generalized solutions, uniqueness of these solutions, and existence for a particular subcase (namely, the case where the diffusion does *not* involve a discontinuous parameter) by a convergence proof for a simple upwind difference scheme. The results imply that for that particular subcase, which is generated by the assumption that driver anticipation and reaction is not altered by abrupt changes of the road surface conditions, the model is well posed. Section 4 presents a selection of numerical examples that permit comparisons between different models discussed in this paper.

2. Mathematical Model

2.1. **Choices of the flux density function.** The flux density function $f(\rho)$ is defined by the velocity function $V(\rho)$. Common examples besides (1.5) are listed in [15] and include the Greenberg model

$$V(\rho) = V_{\mathrm{GB}}(\rho) = \ln(\rho_{\max}/\rho), \tag{2.1}$$

Underwood's model

$$V(\rho) = V_{\mathrm{U}}(\rho) = \exp(-\rho/\rho_{\mathrm{opt}}), \tag{2.2}$$

where $\rho_{\rm opt}$ is an optimum density [25] and which has been used as a model for low densities, Greenshield's model

$$V(\rho) = V_{\rm GS}(\rho) = 1 - (\rho/\rho_{\max})^n \tag{2.3}$$

and the California model

$$V(\rho) = V_{\rm CA}(\rho) = \frac{1}{\rho} - \frac{1}{\rho_{\max}} \tag{2.4}$$

fitting best for heavy traffic. Extensive comparisons of these models and their experimental support is provided in [12, 25]. These models are stated here to clarify which of these models are included in our analysis, and which are not. We require that the function $f(\rho)$ is Lipschitz continuous and compactly supported in the interval $[0, \rho_{\max}]$ All these assumptions are satisfied by the functions $f(\rho)$ defined by (1.4) if the model functions $V(\rho)$ given by (2.1), (2.3) or (2.4) are used, but we may also include models that lead to flux functions (ρ) that are not necessarily convex, such as (2.2). For that particular example, some modification has to be made near $\rho = \rho_{\max}$ in order to achieve compact support. A compactly supported, continuous modification of the function $f_{\rm U}(\rho) := \rho V_{\rm U}(\rho)$ can be constructed if we note first that $f_{\rm U}(\rho)$ has a local maximum at $\rho_{\rm M} = \rho_{\rm opt}$ and an inflection point at $\rho_{\rm infl} = 2\rho_{\rm opt}$. Then we consider the alternative function

$$V_{\rm UA}(\rho) := (1 - \rho/\rho_{\max})^N, \quad f_{\rm UA}(\rho) := \begin{cases} \rho V_{\rm UA}(\rho) & \text{for } 0 \le \rho \le \rho_{\max}, \\ 0 & \text{otherwise,} \end{cases} \tag{2.5}$$

which for $N > 0$ has compact support on $(0, \rho_{\max})$ and is continuous. Moreover, for $N > 1$ this function has a local maximum at $\rho_{\rm M} = \rho_{\max}/(1+N)$ and and an inflection point at $\rho_{\rm infl} = 2\rho_{\rm M} = 2\rho_{\max}/(1+N)$. Consequently, these points coincide with those of the original function $f_{\rm U}(\rho)$ if we choose the exponent

$$N = \frac{\rho_{\max}}{\rho_{\rm opt}} - 1. \tag{2.6}$$

This works if $\rho_{\rm opt} < \rho_{\max}/2$, which is the case in the example considered in Section 4. Furthermore, in the dilute limit $\rho \downarrow 0$ both functions have the same tangent, since

$$\lim_{\rho \to 0^+} f'_{\rm U}(\rho) = \lim_{\rho \to 0^+} f'_{\rm UA}(\rho) = 1.$$

It should be mentioned that Mochon's [26] and Nelson's [28] analyses are based on the assumption of concavity ($f''(\rho) < 0$ for $0 \le \rho \le \rho_{\max}$), a condition that we do not impose here.

2.2. **Discontinuous road surface condition.** Mochon [26] introduced the idea that the LWR model can be extended to include abruptly changing road surface conditions by considering that the factor $v_{\max}$ appearing in (1.3) no longer is a constant but depends discontinuously on the location x, i.e. $v_{\max} = v_{\max}(x)$. For example, assume that the largest part of the highway, for simplicity identified here with a real axis, admits a velocity $v^0_{\max}$, and that there is one road segment $[a, b]$ experiencing heavy rainfall or fog (or which has bad pavement), which enforces a reduction of the maximum velocity to a value $v^*_{\max} < v^0_{\max}$. Alternatively, we could assume that the segment $[a, b]$ permits a higher maximum velocity $v^*_{\max} > v^0_{\max}$. Thus, we consider

$$v_{\max}(x) = \begin{cases} v^0_{\max} & \text{for } x < a \text{ and } x > b, \\ v^*_{\max} & \text{for } x \in (a, b), \end{cases} \tag{2.7}$$

$$v^*_{\max} < v^0_{\max} \text{ (Case A) or } v^*_{\max} > v^0_{\max} \text{ (Case B).}$$

In order to be consistent with the many new analyses of conservation laws (and related equations) with discontinuous flux, see e.g. [6, 7, 18, 19, 20], we let $\gamma(x) := v_{\max}(x)$ and rewrite the conservation law (1.2) modified by the road surface change condition (2.7) as

$$\partial_t \rho + \partial_x\big(\gamma(x) f(\rho)\big) = 0, \quad x \in \mathbb{R},\ t > 0. \tag{2.8}$$

Of course, we may also assume that our highway follows a gently shaped landscape with gradients, which leads to a smoothly varying function $v_{\max}(x)$, and therefore a smoothly varying coefficient

function $\gamma(x)$ in (2.8). This situation will not be included here, since its treatment falls within the standard theory of conservation laws with smoothly varying x-dependent flux functions.

2.3. **The diffusively corrected kinematic-wave model.** The basic assumption $v = v(\rho)$ of the LWR traffic flow model states that drivers adjust their velocity instantaneously to the local density. This is a strong simplifying assumption whose validity has been seriously questioned, starting by concerns raised by Lighthill and Whitham themselves [24]. We follow here an amendment to this situation proposed in the present form by Nelson [27], who argues that it is natural to assume that a more realistic model should incorporate a reaction time τ, representing drivers' delay in their response to events, and that this delay is partially compensated by an anticipating distance L, i.e., drivers adjust their velocity to the density seen a distance L ahead. Consequently, if we first take into account the anticipation length only, the instantaneous velocity v at a point (x,t) is no longer given by $v(x,t) = v_{\max}V(\rho(x,t))$, as stated by (1.3); rather, the velocity function $V(\rho(\cdot,\cdot))$ is evaluated not at the point x, but at $x+L$. Finally, we include the reaction time, which means that we replace the argument t by $t-\tau$, and reduce the argument $x+L$ by the distance $v_{\max}V\tau$ traveled in an interval of length τ, see [27] for further explanation and details. These considerations result in the expression

$$v(x,t) = v_{\max}V\big(\rho(x+L-v_{\max}V\tau, t-\tau)\big). \tag{2.9}$$

Note that the notation in (2.9) is ambiguous, since we are not specific about the argument of V inside (2.9). To turn (2.9) into a usable flux expression, we expand $V(\rho(x+L-v_{\max}V\tau,t-\tau))$ around $\rho(x,t)$. Writing ρ for $\rho(x,t)$, we obtain

$$\begin{aligned} V\big(\rho(x+L-v_{\max}V\tau,t-\tau)\big) &= V(\rho) + V'(\rho)\big(\partial_x\rho\cdot(L-v_{\max}V(\rho)) + \partial_t\rho\cdot(-\tau)\big) + \mathcal{O}(\tau^2+L^2) \\ &= V(\rho) + V'(\rho)\big(L\partial_x\rho - \tau\big\{\partial_t\rho + v_{\max}V(\rho)\partial_x\rho\big\}\big) + \mathcal{O}(\tau^2+L^2). \end{aligned}$$

Using the conservation law $\partial_t\rho + \partial_x(v_{\max}\rho V(\rho)) = 0$, we may replace the expression in curled brackets by $-\rho v_{\max}V'(\rho)\partial_x\rho$. This leads to

$$V\big(\rho(x+L-v_{\max}V\tau,t-\tau)\big) = V(\rho) + V'(\rho)\big(L+\tau\rho v_{\max}V'(\rho)\big)\partial_x\rho + \mathcal{O}(\tau^2+L^2). \tag{2.10}$$

We here assume that all functions involved are sufficiently smooth. Inserting (2.10) into (2.9) and multiplying the result by ρ, we get

$$\rho v = v_{\max}\big[\rho V(\rho) + \rho V'(\rho)\big(L+\tau\rho v_{\max}V'(\rho)\big)\partial_x\rho\big] + \mathcal{O}(\tau^2+L^2). \tag{2.11}$$

The reaction length L can also be considered to depend on $v(\rho)$, i.e., $L = L(\rho) = L(v(\rho))$, see [28]. Neglecting the $\mathcal{O}(\tau^2+L^2)$ term and inserting the right-hand side of (2.11) into the conservation equation (1.1), we obtain the convection-diffusion equation

$$\partial_t\rho + \partial_x f(\rho) = \partial_x^2\tilde{D}(\rho), \quad x\in\mathbb{R},\ t>0, \tag{2.12}$$

where $f(\rho)$ is given by (1.4) and the diffusion term is given by

$$\tilde{D}(\rho) := \int_0^\rho -sv_{\max}V'(s)\big(L(s)+\tau v_{\max}sV'(s)\big)\,ds.$$

Finally, we assume that there exists a critical density value $0\le\rho_{\mathrm{c}}\le\rho_{\max}$, up to which the diffusion effect is not present. Thus, the equation we finally state is

$$\partial_t\rho + \partial_x f(\rho) = \partial_x^2 D(\rho), \quad x\in\mathbb{R},\ t>0, \tag{2.13}$$

where for simplicity we suppress dependence on the parameters τ and L, and

$$D(\rho) := \int_0^\rho d(s)\,ds, \qquad d(\rho) := \begin{cases} 0 & \text{if } \rho\le\rho_{\mathrm{c}}, \\ -\rho v_{\max}V'(\rho)\big(L(\rho)+\tau v_{\max}\rho V'(\rho)\big) & \text{if } \rho>\rho_{\mathrm{c}}. \end{cases} \tag{2.14}$$

We emphasize that there are at least two possible motivations for postulating the existence of a critical density ρ_{c}. One of them is offered by Nelson [28] and is based on using the particular Dick-Greenberg [10, 13] model postulating the equation

$$V(\rho) = V_{\mathrm{DG}}(\rho) = \min\big\{1, C\ln(\rho_{\max}/\rho)\big\}, \tag{2.15}$$

where C is a parameter. Obviously, we have

$$V'_{\mathrm{DG}}(\rho) = 0 \quad \text{for } \rho \le \rho_{\mathrm{c}} := \rho_{\max}\exp(-1/C),$$

so that setting $V(\rho) = V_{\mathrm{DG}}(\rho)$ we see that (2.14) is satisfied. A more general viewpoint advanced, for example, in [30] is that ρ_{c} is a threshold value in the sense that the drivers' reaction can be considered instantaneous in relatively free traffic flow, i.e. when $\rho \le \rho_{\mathrm{c}}$, and otherwise is modeled by the diffusion term. These two viewpoints are different in origin, but give rise to the same behaviour of the diffusion coefficient. We assume that the function $V(\rho)$ is chosen such that $\tilde{d}(\rho) > 0$ for $\rho_{\mathrm{c}} < \rho < \rho_{\max}$. Consequently, the right-hand side of (2.13) vanishes on the interval $[0, \rho_{\mathrm{c}}]$, and possibly at the maximum concentration $\rho_{\max}$. Thus, (2.13) is a second-order parabolic quasilinear partial differential equation that degenerates into first-order hyperbolic type for $\rho \in [0, \rho_{\mathrm{c}}]$. Since the degeneracy takes place on a solution interval of positive length, we call (2.13) strongly degenerate parabolic.

Finally, we point out that Nelson [28] suggests a dependence $L = L(v(\rho))$ of the following type:

$$L = \max\left\{\frac{(v(\rho))^2}{2a}, L_{\min}\right\}, \tag{2.16}$$

where the first argument is the distance required to decelerate to full stop from speed $v(\rho)$ at deceleration a, and the second imposes the assumption of a minimal anticipation distance, regardless of how small the velocity is.

2.4. **The combined diffusively corrected kinematic-wave model with changing road surface conditions.** So far we have had separate looks at the effect of changing road surface conditions, which introduces a discontinuous coefficient in the convective flux function, and the inclusion of drivers' anticipation and reaction, which gives rise to a degenerating diffusion term. These two modifications of the LWR model are independent, and we may combine them into one new equation that we suggest for traffic flow with drivers' anticipation *and* changing road surface conditions. We will do so by admitting two variants, referred to as 'Model 1' and 'Model 2'.

Model 1 is based on the viewpoint that the diffusion term models (though possibly in a very gross manner) 'driver psychology' and should therefore be independent of road surface conditions. Thus, we will assume for Model 1 that the 'combined' model is produced by replacing $f(\rho)$ in (2.13) by the expression $\gamma(x)f(\rho)$ appearing in (2.8), but that at the same time the drivers' anticipation behaviour is determined by some constant value $v_{\max}$, for example the 'default' value $v^0_{\max}$ in (2.7).

The more involved Model 2 corresponds to the conclusion that the ingredients set out in Sections 2.2 and 2.3 can be combined if we go again through the derivation of equation (2.13) and simply replace every occurrence of $v_{\max}$ by $v_{\max}(x)$. To derive Model 2, note first that the expansion (2.11) remains valid if we replace the constant $v_{\max}$ by $v_{\max}(x)$, even when $v_{\max}$ is discontinuous. Then it is straightforward to conclude that the resulting strongly degenerate convection-diffusion equation is given as

$$\partial_t\rho + \partial_x\big(\gamma(x)f(\rho)\big) = \partial_x^2 D_2\big(\rho, \gamma(x)\big), \quad x \in \mathbb{R},\ t > 0, \tag{2.17}$$

where we recall the notation $\gamma(x) = v_{\max}(x)$ and define

$$D_2\big(\rho, \gamma(x)\big) := \int_0^\rho \hat{d}\big(s, \gamma(x)\big)\, ds, \tag{2.18}$$

$$\hat{d}\big(\rho, \gamma(x)\big) := \begin{cases} 0 & \text{for } \rho \le \rho_{\mathrm{c}}, \\ \gamma(x)r\big(\rho; \tau, L(\rho, \gamma(x))\big) & \text{for } \rho > \rho_{\mathrm{c}}. \end{cases} \tag{2.19}$$

Note that the anticipation length L is in general assumed to depend on $v(\rho)$. Thus, if that velocity depends on $\gamma(x)$, then so will L, which we denote by $L = L(\rho, \gamma(x))$. Observe that the use of (2.16), for example, implies that $D_1(x)$ depends nonlinearly on $\gamma(x)$.

Model 1 leads to the simpler strongly degenerate convection-diffusion equation

$$\partial_t\rho + \partial_x\big(\gamma(x)f(\rho)\big) = \partial_x^2 D_1(\rho), \quad x \in \mathbb{R},\ t > 0, \tag{2.20}$$

with $D_1(\rho) := D_2(\rho, v^0_{\max})$. Recall that the function $f(\rho)$ and the coefficient $\gamma(x)$ are nonnegative.

To retain only the essential functional dependencies in the notation, observe that we can write $D_2 = \gamma(x)R(\rho, \gamma(x))$, where

$$R\big(\rho, \gamma(x)\big) := \frac{1}{\gamma(x)} \int_0^\rho d\big(s, \gamma(x)\big)\, ds.$$

Then combine the two models into the single equation

$$\partial_t \rho + \partial_x \big(\gamma^1(x) f(\rho)\big) = \partial_x \big(\gamma^2(x) \partial_x R(\rho, \gamma^2(x))\big), \tag{2.21}$$

where $\gamma^1(x) := \gamma(x) = v_{\max}(x)$ for both models, $\gamma^2 \equiv v^0_{\max}$ for Model 1 and $\gamma^2(x) := \gamma(x)$ for Model 2, where $v^0_{\max}$ and the function $v_{\max}(x)$ are defined in (2.7). For simplicity of the discussion, we assume that $[a, b] = [0, 1]$, and consider a prescribed initial car density

$$\rho(x, 0) = \rho_0(x), \quad x \in \mathbb{R}. \tag{2.22}$$

We admit here the special choice $L = \tau = 0$, for which the right-hand part of (2.21) vanishes identically and the first-order equation (2.8) is recovered. The remainder of this paper is concerned with the analysis and discretization of the initial value problem (2.21), (2.22).

3. Mathematical theory

In [18, 20] a rather general well-posedness (existence and uniqueness) theory is developed for strongly degenerate convection-diffusion equations with discontinuous coefficients. Since in [18, 20] the diffusion function is not allowed to depend on x, the remainder of this section is therefore concerned with the initial value problem (2.20), (2.22) for Model 1. Having said this, it seems likely that the analysis in [18, 20] can be extended to the x-dependent diffusion case (2.21).

The purpose of this section is recall the main results of theory developed in [18, 20] as it applies to Model 1, under the following assumptions on the initial car density ρ_0:

$$\begin{cases} \rho_0 \in L^1(\mathbb{R}) \cap BV(\mathbb{R}); \quad \rho_0(x) \in [0, \rho_{\max}] \ \forall x \in \mathbb{R}; \\ A(\rho_0) \text{ is absolutely continuous on } \mathbb{R}; \\ A(\rho_0)_x \in BV(\mathbb{R}). \end{cases} \tag{3.1}$$

The assumption that $A(\rho_0)$ is absolutely continuous implies that any jump in ρ_0 must be contained within the interval $[0, \rho_c]$. However, this is a technical condition for the mathematical and convergence analysis to work, but that there is no problem in taking more general initial conditions for the numerical simulations, as we do in Section 4.

We refer to [18, 20] for a historical account on conservation laws and degenerate parabolic equations with discontinuous coefficients.

Independently of the smoothness of the coefficient $\gamma(x) = v_{\max}(x)$ describing the road conditions, solutions to (2.20), (2.22) will in general not be smooth. In fact, they can be discontinuous since $D_1'(\rho)$ is zero for $\rho \le \rho_c$. Therefore it becomes necessary to interpret (2.20), (2.22) in the weak (distributional) sense in order to make sense to the solutions. Moreover, as is well known in the context of conservation laws [4, 8, 16], weak solutions are not unique and one needs an additional condition, the entropy condition, to single out a unique solution.

We denote by $\mathcal{M}(\Pi_T)$ the finite Radon (signed) measures on Π_T. The space $BV(\Pi_T)$ of functions of bounded variation is defined as the set of locally integrable functions $W : \Pi_T \to \mathbb{R}$ for which $\partial_x W, \partial_t W \in \mathcal{M}(\Pi_T)$. In this paper we use the space $BV_t(\Pi_T)$ of locally integrable functions $W : \Pi_T \to \mathbb{R}$ for which only $\partial_t W \in \mathcal{M}(\Pi_T)$. Of course, we have $BV(\Pi_T) \subset BV_t(\Pi_T)$. We can also define the space $BV_x(\Pi_T)$ by replacing the condition $\partial_t W \in \mathcal{M}(\Pi_T)$ by $\partial_x W \in \mathcal{M}(\Pi_T)$. Moreover, we denote by $\mathcal{D}(\Pi_T)$ the space of test functions on Π_T that vanish for $t = 0$ and $t = T$, i.e., $\mathcal{D}(\Pi_T) = C_0^\infty(\mathbb{R} \times (0, T))$.

Equipped with these definitions, we can state the notion of entropy solution suggested in [18, 20] and translated to our setting as follows:

Definition 3.1 (BV_t entropy solution)**.** *Let $\Pi_T = \mathbb{R} \times (0, T)$ with $T > 0$ fixed. A function $u : \Pi_T \to \mathbb{R}$ is a BV_t entropy solution of the initial value problem* (2.20), (2.22) *on Π_T if it satisfies the following conditions:*

(**D**.1) $\rho \in L^1(\Pi_T) \cap BV_t(\Pi_T)$ *and* $\rho(x,t) \in [0, \rho_{\max}]$ *for a.e.* $(x,t) \in \Pi_T$.

(**D**.2) $D_1(\rho)$ *is continuous and* $D_1(\rho)_x \in L^\infty(\Pi_T)$.

(**D**.3) *For all* $c \in \mathbb{R}$ *and all* $0 \le \phi \in \mathcal{D}(\Pi_T)$*:*

$$\begin{aligned} &\iint_{\Pi_T} \Big(|\rho - c|\, \phi_t + \operatorname{sgn}(\rho - c)\gamma(x)(f(\rho) - f(c))\phi_x + |D_1(\rho) - D_1(c)|\, \phi_{xx} \Big)\, dt\, dx \\ &\quad + \int_0^T \left| v^0_{\max} - v^*_{\max} \right| f(c)\, (\phi(a,t) + \phi(b,t))\ dt \ge 0. \end{aligned} \tag{3.2}$$

(**D**.4) *The initial condition is satisfied in the following strong* L^1 *sense:*

$$\operatorname*{ess\,lim}_{t \downarrow 0} \int_{\mathbb{R}} |\rho(x,t) - \rho_0(x)|\ dx \to 0.$$

It is not difficult to see that the entropy condition (**D**.4) implies that (2.20) also holds in the weak sense. It is well known that there exists an entropy solution to (2.20), (2.22) on Π_T if the road conditions $\gamma(x)$ depend smoothly on x, and this solution belongs to $BV(\Pi_T)$ under our assumptions (3.1) on the initial car density ρ_0, see [31]. However, in our context with $\gamma(x)$ depending discontinuously on x, it is hard (if possible) to prove that solutions belong to $BV_x(\Pi_T)$. It is, however, possible to prove that there exist solutions that belong to $BV_t(\Pi_T)$, and this motivates the BV_t requirement in (**D**.1).

The following theorem is taken from [20]. It states that the BV_t entropy solution is stable with respect to the L^1 norm and is uniquely determined by its initial data:

Theorem 1 (L^1 stability and uniqueness)**.** *Let* ρ_1*,* ρ_2 *be two* BV_t *entropy solutions to* (2.20)*,* (2.22) *on* Π_T *with initial data* $\rho_{1,0}$*,* $\rho_{2,0}$ *satisfying* (3.1)*. Then for a.e.* $t \in (0,T)$

$$\|\rho(\cdot,t) - \rho(\cdot,t)\|_{L^1(\mathbb{R})} \le \|\rho_0 - \rho_0\|_{L^1(\mathbb{R})}. \tag{3.3}$$

In particular, there exists at most one BV_t *entropy solution of* (2.20)*,* (2.22)*.*

The proof of Theorem 1 can be found in [20]. Let us here only recall that it relies on jump conditions that relate limits from the right and left of the BV_t entropy solution $\rho(\cdot,t)$ at $x = a, b$ (the two points where the coefficient describing the road conditions has jump discontinuities). To be more precise, we use a Rankine-Hugoniot condition expressing conservation across the jumps at $x = a, b$, and also an entropy jump inequality which is a consequence of the entropy condition (3.2). Let $\xi = a$ or b, and introduce the notations

$$\begin{aligned} &\gamma_\pm := \gamma(\xi\pm), \qquad \rho_\pm := \rho_\pm(t) := \rho(\xi_m\pm, t), \\ &\mathcal{D}_{1,\pm} := \mathcal{D}_{1,\pm}(t) := \mathcal{D}_1(\xi_m\pm, t), \qquad \mathcal{D}_1(x,t) := D_1(\rho)_x(x,t). \end{aligned}$$

The existence of the above limits (traces) is not entirely obvious since Definition 3.1 says nothing about the regularity of $\rho(x,t)$ in the x variable. Nevertheless, in [20] it is proved that the above traces exist due to the entropy condition (3.2) and the assumption that $\rho \in BV_t(\Pi_T)$, i.e., $u_t \in L^1(\Pi_T)$. Equipped with the existence of these traces, one can easily prove that the following Rankine-Hugoniot jump condition holds for a.e. $t \in (0,T)$:

$$\gamma_+ f(\rho_+) - \mathcal{D}_{1,+} = \gamma_- f(\rho_-) - \mathcal{D}_{1,-}. \tag{3.4}$$

In addition, the following entropy jump condition holds for every $c \in \mathbb{R}$ and for a.e. $t \in (0,T)$:

$$\begin{aligned} &\big(\gamma_+ F(\rho_+, c) - \operatorname{sgn}(\rho_+ - c)\mathcal{D}_{1,+}\big) \\ &\quad - \big(\gamma_- F(\rho_-, c) - \operatorname{sgn}(\rho_- - c)\mathcal{D}_{1,-}\big) \le \left| v^0_{\max} - v^*_{\max} \right| f(c), \end{aligned} \tag{3.5}$$

where $F(u,v) = \operatorname{sgn}(u - v)(f(u) - f(v))$ denotes the Kružkov entropy flux. The jump conditions (3.4) and (3.5) are essential ingredients in the uniqueness proof in [20].

The next theorem is taken from [18] and states that there exists a BV_t entropy solution. Together with Theorem 1, this shows that our Model 1 is mathematically well posed.

Theorem 2 (existence)**.** *Suppose that* (3.1) *holds. Then there exists a BV_t entropy solution $\rho(x,t)$ to the initial value problem* (2.20)*,* (2.22)*.*

The proof this existence theorem is constructive and is based on proving convergence (compactness) of an explicit finite difference scheme. Let us state a generalization of this finite difference that applies to (2.21), not just (2.20). This scheme will be used in Section 4 for computational purposes. The difference scheme for (2.21), (2.22) is a straightforward extension of the scheme analyzed in [18] (see also [20]) to the case where the diffusion term also includes a discontinuous coefficient. To define the scheme, we choose a discretization $\Delta x > 0$, set $x_j := j\Delta x$, and discretize the parameter vector $\boldsymbol{\gamma}(x) := (\gamma^1(x), \gamma^2(x))$ and the initial datum $\rho_0(x)$ by

$$\boldsymbol{\gamma}_{j+1/2} := \boldsymbol{\gamma}\left(\hat{x}_{j+1/2}+\right), \quad \rho_j^0 := \frac{1}{\Delta x}\int_{x_{j-1/2}}^{x_{j+1/2}} \rho_0(x)\,dx, \quad j \in \mathbb{Z},$$

where $\hat{x}_{j+1/2}$ is any point lying in the interval $I_{j+1/2} = (x_j, x_{j+1})$.

Observe that the spatial discretization of the discontinuity parameter vector $\boldsymbol{\gamma}$ is staggered against that of the conserved variable ρ. We choose Δt, set $\lambda := \Delta t/\Delta x$, $\mu = \Delta t/(\Delta x)^2$, and for $n > 0$ define the approximations $\{\rho_j^n\}_{j,n}$, $\rho_j^n \approx \rho(x_j, t_n)$ with $\rho(x,t)$ solving the combined model (2.21), (2.22), according to the explicit marching formula

$$\rho_j^{n+1} = \rho_j^n - \Delta_-\Big(\lambda\gamma_{j+1/2}^1 f^{\mathrm{EO}}\big(\rho_{j+1}^n, \rho_j^n\big) - \mu\gamma_{j+1/2}^2\Delta_+ R\big(\rho_j^n, \gamma_{j-1/2}^2\big)\Big), \tag{3.6}$$

where the numerical (Engquist-Osher) flux [11] is given by

$$f^{\mathrm{EO}}(v,u) := \frac{1}{2}\left[f(u) + f(v) - \int_u^v \big|f'(s)\big|\,ds\right]. \tag{3.7}$$

We use Δ_+ and Δ_- to denote the forward and backward difference operators in the x direction, for example, $\Delta_+\rho_j^n = \rho_{j+1}^n - \rho_j^n = \Delta_-\rho_{j+1}^n$.

For (2.20), (2.22) (Model 1), the scheme (3.6) simplifies to

$$\rho_j^{n+1} = \rho_j^n - \Delta_-\Big(\lambda\gamma_{j+1/2} f^{\mathrm{EO}}\big(\rho_{j+1}^n, \rho_j^n\big) - \mu\Delta_+ D_1\big(\rho_j^n\big)\Big). \tag{3.8}$$

This is the difference scheme that is discussed below.

Finally, we let $t_n := n\Delta t$, and let χ^n and χ_j denote the characteristic functions of $[t_n, t_{n+1})$ and $[x_{j-1/2}, x_{j+1/2})$, respectively, and define the following approximations of the solution and of the parameter vector, where Δ is a collective symbol for the discretization parameters Δx, Δt:

$$\rho^\Delta(x,t) := \sum_{n>0}\sum_{j\in\mathbb{Z}} \rho_j^n \chi_j(x)\chi^n(t), \quad \gamma^\Delta(x) := \sum_{j\in\mathbb{Z}} \gamma_{j+1/2}\chi_{j+1/2}(x).$$

This means that $\rho^\Delta = \rho_j^n$ and $\gamma^\Delta = \gamma_{j+1/2}$ on the rectangle $[x_{j-1/2}, x_{j+1/2}) \times [t_n, t_{n+1})$ and on the interval $[x_{j-1/2}, x_{j+1/2})$, respectively.

According to [18, 20], the proof of Theorem 2 consists in establishing two main parts: (i) compactness of the sequence $\{\rho^\Delta\}_{\Delta>0}$, i.e., that there exists at least a subsequence that converges in $L^1_{\mathrm{loc}}(\Pi_T)$ to limit function ρ and (ii)satisfaction of the entropy condition (3.2) by the limit ρ. Then Theorem 1 (uniqueness) implies that the whole sequence $\{\rho^\Delta\}_{\Delta>0}$ (not just some subsequence of it) converges in $L^1_{\mathrm{loc}}(\Pi_T)$ to the BV_t entropy solution of (2.20), (2.22).

For the convenience of the reader we sketch in some more detail the main steps of (i) and (ii). First of all, the difference scheme (3.8) is monotone, which means that if the scheme is written in the form

$$\rho_j^{n+1} = G_j\big(\rho_{j+1}^n, \rho_j^n, \rho_{j-1}^n, \boldsymbol{\gamma}_{j-1/2}, \boldsymbol{\gamma}_{j+1/2}\big),$$

then $\partial\rho_j^{n+1}/\partial\rho_{j+k}^n = \partial G_j/\partial\rho_{j+k}^n \geq 0$ for $k = -1, 0, 1$. The monotonicity property can be easily verified. See also [18, Lemma 3.2]. Moreover, we have that $\rho_j^n \in [0, \rho_{\max}]$ for all j, n if the following CFL condition holds:

$$\lambda \max\big(v_{\max}^0, v_{\max}^*\big) \max_{[0,\rho_{\max}]}|f'| + \mu \max_{[0,\rho_{\max}]}|D_1'| \leq \frac{1}{2}. \tag{3.9}$$

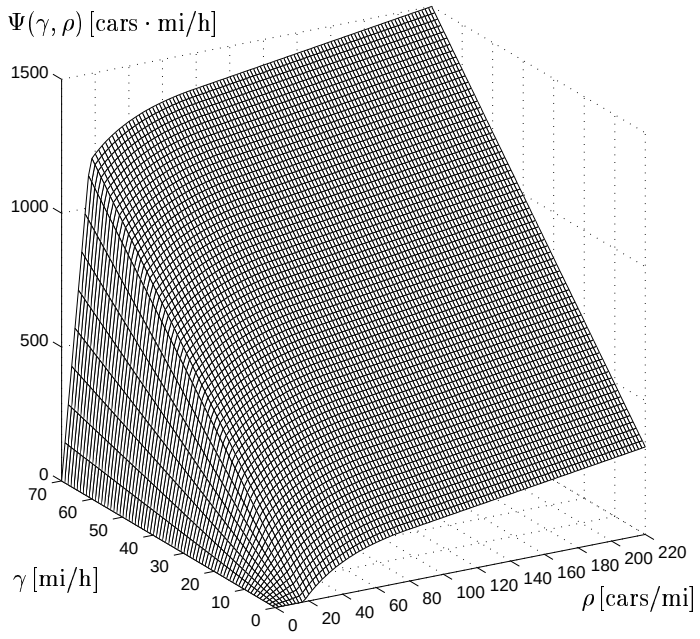

FIGURE 1. An example of the singular mapping $\Psi(\gamma,\rho)$. The corresponding functions $f(\rho)=f_{\mathrm{DG}}(\rho)$ and $D_1(\rho)$ are given in Section 4.

An important consequence of monotonicity is L^1 time continuity of the numerical approximations, which means that is there exists a constant C, independent of Δ, such that for any integer $n\geq 0$

$$\Delta x\sum_j\left|\rho_j^{n+1}-\rho_j^n\right|\leq\Delta x\sum_j\left|\rho_j^1-\rho_j^0\right|\leq C\Delta t. \tag{3.10}$$

It is not possible to derive a corresponding estimate in space since the parameter γ is discontinuous (see [18] for a discussion of this point), but (3.10) plays a key role in deriving a bound on the space translates of a certain transformed variable (the so-called singular mapping $\Psi(\gamma,\rho)$). In passing, we note that (3.10) will ensure that any the limit of $\{\rho^\Delta\}_{\Delta>0}$ belongs to $BV_t(\Pi_T)$.

The singular mapping $\Psi(\gamma,\rho)$ in [18] is designed to be Lipschitz continuous in both variables and strictly increasing as a function of ρ, and it reads

$$\Psi(\gamma,\rho)=\gamma\int_0^\rho\mathcal{S}(\xi)\left|f'(\xi)\right|\,d\xi+D_1(\rho)=:\mathcal{F}(\gamma,\rho)+D_1(\rho), \tag{3.11}$$

where the indicator function $S(\xi)$ is 1 if $\xi\in[0,\rho_{\mathrm{c}}]$ and 0 otherwise. The singular mapping zeroes out the contribution of the convective flux wherever $D_1(\rho)$ is non-degenerate. Note that

$$\frac{\partial}{\partial\rho}\Psi(\gamma,\rho)=\begin{cases}\gamma\left|f'(\rho)\right| & \text{for } \rho\in[0,\rho_{\mathrm{c}}],\\ D_1'(\rho) & \text{for } \rho\in(\rho_{\mathrm{c}},\rho_{\max}],\end{cases}$$

so that $\partial\Psi(\gamma,\rho)\partial\rho>0$ for a.e. $\rho\in[0,\rho_{\max}]$ and hence $\rho\mapsto\Psi(\gamma,\rho)$ is is strictly increasing. For a specific choice of the functions $f(\rho)$ and $D_1(\rho)$ to be introduced later, the mapping $\Psi(\gamma,\rho)$ is plotted in Figure 1.

Introduce the transformed quantity

$$z^\Delta(x,t):=\Psi(\gamma,\rho^\Delta(x,t)).$$

The strategy is to prove L^1 convergence along a subsequence of $\{z^\Delta\}_{\Delta>0}$. Note that this also implies convergence of $\{\rho^\Delta\}_{\Delta>0}$ since $\rho\mapsto\Psi(\gamma,\rho)$ is invertible. To prove convergence of $\{z^\Delta\}_{\Delta>0}$,

[18] proceeds in two separate steps: (a) Convergence of the diffusion part of $\Psi(\gamma,\rho)$, namely $D_1^\Delta(x,t) := D_1(\rho^\Delta)$. (b) Convergence of the hyperbolic part of Ψ, namely $\mathcal{F}^\Delta(x,t) := \mathcal{F}(\gamma^\Delta,\rho^\Delta)$.

Step (a) is achieved by an energy argument, which implies that $\{D_1^\Delta(x,t)\}_{\Delta>0}$ converges along a subsequence a.e. and in $L^2_{\mathrm{loc}}(\Pi_T)$ to a limit $\overline{D_1} \in L^2(0,T;H^1(\mathbb{R}))$. Moreover, $\overline{D_1} = D_1(\rho)$, where ρ is the $L^\infty(\Pi_T)$ weak-$\star$ limit of ρ^Δ. It is possible to improve the regularity of $D_1(\rho)$. From the L^1 time estimate (3.10) the following space estimate follows easily:

$$\left|D_1(\rho_j^n) - D_1(\rho_i^n)\right| \le C\,|j-i|\,\Delta x, \qquad \forall i,j \in \mathbb{Z},$$

for some constant C that is independent of Δ. Although the proof is more involved, one can also prove the following time estimate:

$$\left|D_1(\rho_j^n) - D_1(\rho_j^m)\right| \le C\sqrt{|n-m|\,\Delta t}, \qquad \forall m,n \in \mathbb{N}\cup\{0\},$$

for some constant C that is independent of Δ. These estimates imply eventually that $D_1(\rho)$ is (Hölder) continuous and $D_1(\rho)_x \in L^\infty(\Pi_T)$, i.e., that condition (**D**.2) of Definition 3.1 holds.

Step (b) is achieved by uniformly bounding the total variation of $\mathcal{F}^\Delta(\cdot,t)$ for all $t \in (0,T)$. The proof of this bound relies on a clever use of the following cell entropy inequality satisfied by the difference scheme (3.8) for any integer j, any nonnegative integer n, and any $c \in \mathbb{R}$:

$$\begin{aligned}\left|\rho_j^{n+1} - c\right| \le \left|\rho_j^n - c\right| &- \Delta_-\Big(\lambda\gamma_{j+1/2}F_{j+1/2}^n - \mu\Delta_+\left|D_1\left(\rho_j^n\right) - D_1(c)\right|\Big)\\ &- \lambda\,\mathrm{sgn}\left(\rho_j^{n+1}-c\right)\Delta_-\gamma_{j+1/2}f(c),\end{aligned} \tag{3.12}$$

where the numerical entropy flux $F_{j+1/2}^n$ is defined by

$$F_{j+1/2}^n = f^{\mathrm{EO}}\left(\rho_{j+1}^n \vee c, \rho_j^n \vee c\right) - f^{\mathrm{EO}}\left(\rho_{j+1}^n \wedge c, \rho_j^n \wedge c\right), \tag{3.13}$$

and $a \vee b = \max(a,b)$, $a \wedge b = \min(a,b)$.

In view of (3.10) and the total variation bound on $\mathcal{F}^\Delta$, $\{\mathcal{F}^\Delta\}_{\Delta>0}$ converges along a subsequence to a limit function $\overline{\mathcal{F}}$ a.e. and in $L^1_{\mathrm{loc}}(\Pi_T)$. Compactness of $\{D_1^\Delta(x,t)\}_{\Delta>0}$ and $\{\mathcal{F}^\Delta(x,t)\}_{\Delta>0}$ separately implies the desired compactness of $\{z^\Delta\}_{\Delta>0}$. Let $z(x,t)$ be a limit point of $\{z^\Delta\}_{\Delta>0}$ and define $\rho(x,t) := \Psi^{-1}(\gamma(x),z(x,t))$. It is now possible to prove that this function $\rho(x,t)$ is a BV_t entropy solution to the initial value problem (2.20), (2.22) in the sense of Definition 3.1. In particular, one proves that the entropy condition (3.2) is satisfied by the limit ρ as a consequence of the cell entropy inequality (3.12), exploiting the obvious fact

$$-\lambda\,\mathrm{sgn}\left(\rho_j^{n+1}-c\right)\Delta_-\gamma_{j+1/2}f(c) \le \lambda\left|\Delta_-\gamma_{j+1/2}\right| f(c).$$

We refer to [18, 20] for the complete (but rather long and technical) proofs of Theorems 1 and 2.

4. Numerical examples

To illustrate the mathematical model and performance of the numerical scheme (3.6), we consider a series of eight numerical examples. In the first four examples, we do not take into account driver reaction, which means that we switch off the diffusion term in (2.21) by setting $\tau = L = 0$. Thus, the first-order equation (2.8) is recovered. In the second group of examples, we do take into account the diffusion term. Our main interest is in providing additional numerical examples for the model case studied by Nelson in [28]. Thus, in the second group of examples, we restrict ourselves to a convex flux function $f(\rho)$. The mesh size ratio λ used is stated for each example.

As an example of a convex flux function $f(\rho)$, we choose the velocity function $V_{\mathrm{DG}}(\rho)$ given by (2.15) and utilize the same parameters as in [28], i.e., $\rho_{\max} = 220$ cars/mi and $C = \mathrm{e}/7 = 0.38833$. (Note that in contrast to the corresponding formula (6) in [28], our equation (2.15) does not contain the factor $v_{\max}$.) This leads to the convex flux function

$$f(\rho) = f_{\mathrm{DG}}(\rho) := \begin{cases} \rho & \text{for } 0 \le \rho \le \rho_{\mathrm{c}} = 0.076142\rho_{\max} = 16.7512\ \text{cars/mi},\\ (\mathrm{e}/7)\rho\ln(\rho_{\max}/\rho) & \text{for } \rho_{\mathrm{c}} < \rho \le \rho_{\max},\\ 0 & \text{otherwise.}\end{cases} \tag{4.1}$$

(The term 'convex' refers, of course, to the behaviour of the function on the interval $(0,\rho_{\max})$ only.) Observe that $f_{\mathrm{DG}}(\rho)$ has a local maximum at $\rho_{\mathrm{M}} = \rho_{\max}/\mathrm{e} \approx 80.9335$ cars/mi, see Figure 2.

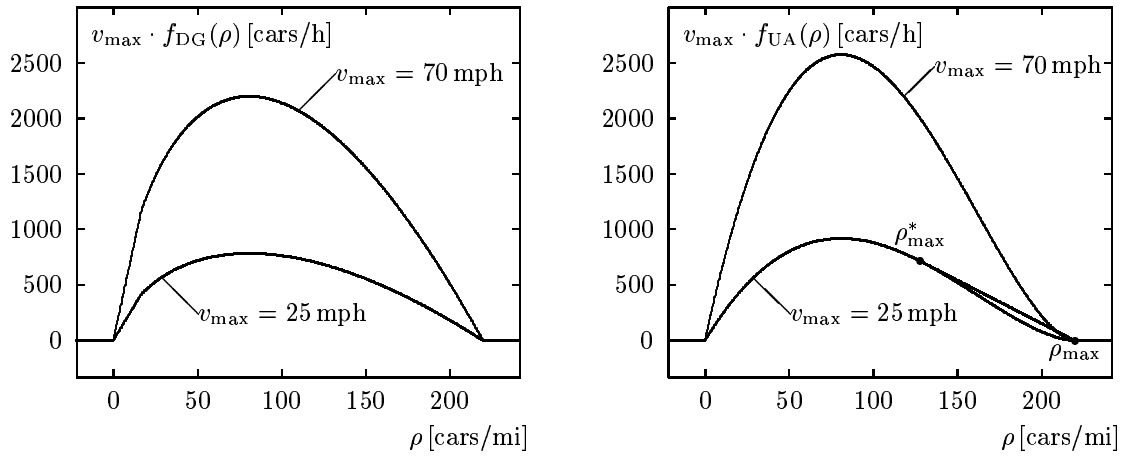

FIGURE 2. The flux functions $v_{\max} f_{\mathrm{DG}}(\rho)$ (left) and $v_{\max} f_{\mathrm{UA}}(\rho)$ (right) for Examples 1 and 2, where $v_{\max} \in \{v^0_{\max} = 25\,\mathrm{mph}, v^*_{\max} = 70\,\mathrm{mph}\}$. The chord joining the points $(\rho^*_{\max}, v^0_{\max} f_{\mathrm{UA}}(\rho^*_{\max}))$ and $(\rho_{\max}, v^0_{\max} f_{\mathrm{UA}}(\rho_{\max}))$ in the right diagram indicates a contact discontinuity forming in Example 2.

For the non-convex case, we choose the functions $V(\rho) = V_{\mathrm{UA}}(\rho)$ and $f(\rho) = f_{\mathrm{UA}}(\rho)$ defined by (2.5) with the same parameter $\rho_{\max} = 220\,\mathrm{cars/mi}$, and let

$$N = \frac{\rho_{\max}}{\rho_{\mathrm{opt}}} - 1 = \frac{\rho_{\max}}{\rho_{\mathrm{M}}} - 1 = \mathrm{e} - 1 = 1.7182\ldots, \tag{4.2}$$

such that the local extrema of $f_{\mathrm{DG}}(\rho)$ and $f_{\mathrm{UA}}(\rho)$ coincide, but $f_{\mathrm{UA}}(\rho)$ also has an inflection point at $\rho_{\mathrm{infl}} = (2/\mathrm{e})\rho_{\max} < \rho_{\max}$; here we get $\rho_{\mathrm{infl}} = 161.867\,\mathrm{cars/mi}$. In both cases, the Engquist-Osher numerical flux function f^{EO} has the explicit representation

$$f^{\mathrm{EO}}(u,v) = \begin{cases} f(u) & \text{if } u \le \rho_{\mathrm{M}} \text{ and } v \le \rho_{\mathrm{M}}, \\ f(\rho_{\mathrm{M}}) & \text{if } u > \rho_{\mathrm{M}} \text{ and } v \le \rho_{\mathrm{M}}, \\ f(u) + f(v) - f(\rho_{\mathrm{M}}) & \text{if } u \le \rho_{\mathrm{M}} \text{ and } v > \rho_{\mathrm{M}}, \\ f(v) & \text{if } u > \rho_{\mathrm{M}} \text{ and } v > \rho_{\mathrm{M}}. \end{cases} \tag{4.3}$$

To be consistent with [28], we choose $v^0_{\max} = 70\,\mathrm{mph}$.

In all numerical examples, we assume that the interval $(a,b) = (0,1)$ corresponds to the road segment with an exceptional maximum velocity. Since we choose the discretization parameter $\Delta x = 1/J$, we have

$$\gamma^1_{j+1/2} = \begin{cases} v^*_{\max} & \text{for } j = 1,\ldots J, \\ v^0_{\max} & \text{otherwise,} \end{cases}$$

and $\gamma^2_{j+1/2} = 0$ for all j in the case of the kinematic model, $\gamma^2_{j+1/2} = v^0_{\max}$ for the diffusively corrected kinematic Model 1, and $\gamma^2_{j+1/2} = \gamma^1_{j+1/2}$ for Model 2.

The first four examples are simulations of the kinematic traffic flow model with changing road surface condition, and the second four refer to the diffusive correction of the same model.

4.1. **Simulations of the kinematic traffic model with changing road surface conditions.**

4.1.1. *Dissolution of a traffic jam (Examples 1 and 2).* Examples 1 and 2 are chosen in such a way that the convex flux-density function $f_{\mathrm{DG}}(\rho)$ and the non-convex function $f_{\mathrm{UA}}(\rho)$ produce different solutions. At the same time, these are the only examples in which we consider Case B, i.e., a finite road segment with an enlarged maximum velocity. Specifically, we assume $v^0_{\max} = 25\,\mathrm{mph}$ and $v^*_{\max} = 70\,\mathrm{mph}$. The resulting four flux functions involved in the numerical examples are plotted in Figure 2.

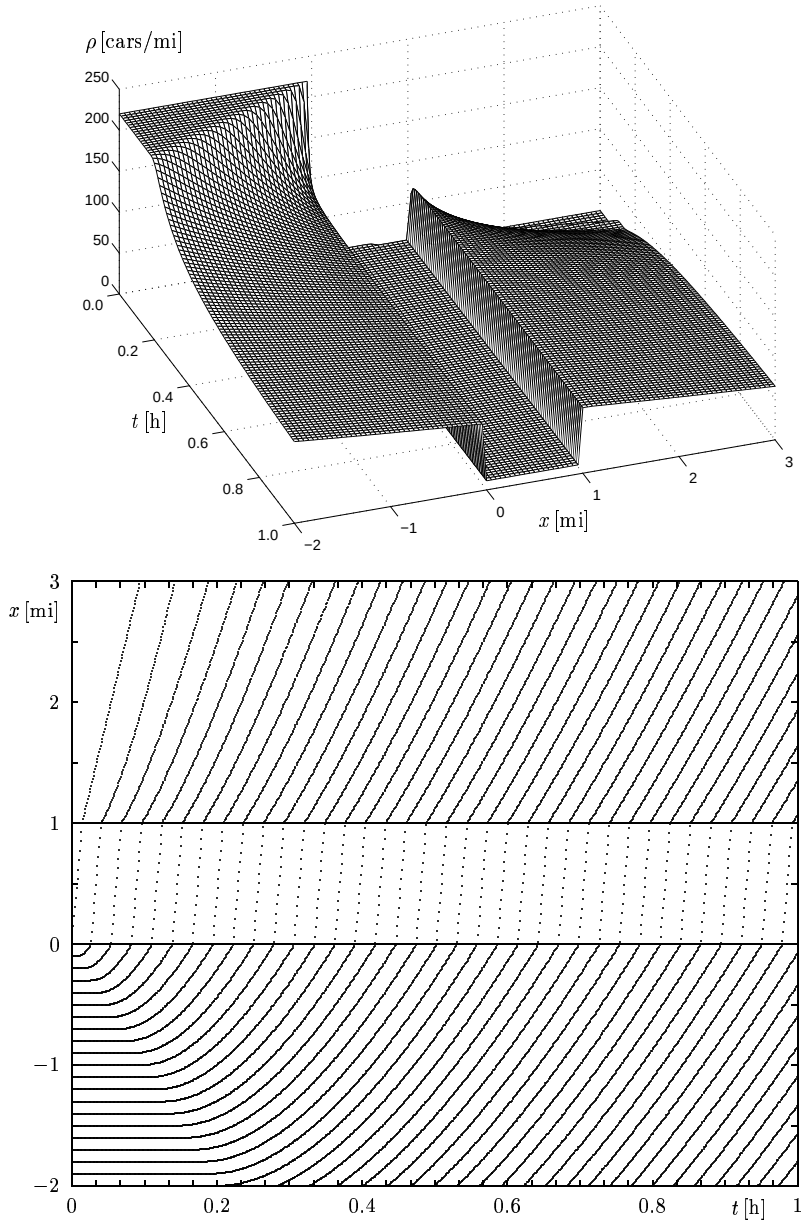

FIGURE 3. Example 1: Dissolution of a traffic jam and effect of a finite road segment with enlarged maximum velocity (Case B): numerical solution $\rho(x,t)$ (top) and car trajectories (bottom), starting from $x_i(0) = -i \cdot 0.25\,\mathrm{mi}$, $i = 1, 2, 3 \ldots$, calculated by using the convex flux density function $f(\rho) = f_{\mathrm{DG}}(\rho)$ given by (4.1).

The initial density is prescribed as

$$\rho_0(x) = \begin{cases} \rho_{\max} = 220\,\mathrm{cars/mi} & \text{for } x < 0, \\ 0 & \text{otherwise.} \end{cases}$$

This datum corresponds to a a very long bumper-to-bumper traffic jam that has formed just at the entrance to the road segment $(0, 1)$, and we may assume that at $t = 0$, a traffic light restricting entry to that segment turns green, and the traffic jam starts to dissolve. Figure 3 shows the

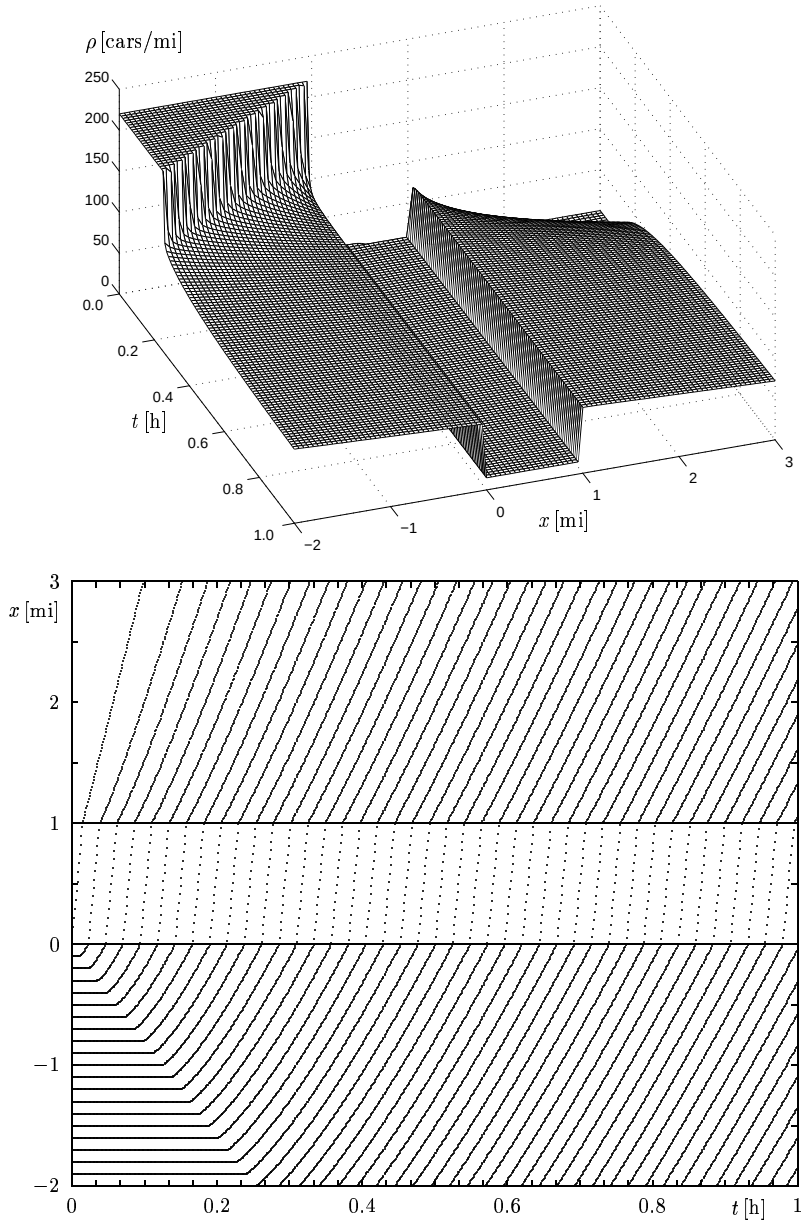

FIGURE 4. Example 2: Dissolution of a traffic jam and effect of a finite road segment with enlarged maximum velocity (Case B): numerical solution $\rho = \rho^{\Delta}(x,t)$ (top) and car trajectories (bottom), starting from $x_i(0) = -i \cdot 0.25\,\mathrm{mi}$, $i = 1, 2, 3 \ldots$, calculated by using the non-convex flux density function $f(\rho) = f_{\mathrm{UA}}(\rho)$ given by (2.5), (4.2).

numerical simulation for the case of the convex flux function $f(\rho) = f_{DG}(\rho)$, both as a plot of the density calculated numerically and as selected car trajectories, while Figure 4 displays the same results for the non-convex flux density function $f(\rho) = f_{\mathrm{UA}}(\rho)$. The numerical solution has been calculated with $\Delta x = 1/200\,\mathrm{mi}$ and $\lambda = 0.002\,\mathrm{h/mi}$. Note that here and in all similar plots in this paper, the visual grid used for the three-dimensional plots of the numerically calculated density is much coarser than the computational. Here and in all cases, we have calculated the car

trajectories from local velocities $v(\rho) = v_{\max} f(\rho)/\rho$, using the numerical solution $\rho = \rho^{\Delta}(x,t)$, starting from the initial positions given in each caption, respectively.

The numerical solutions of both cases display very similar structure and show how the traffic jam starts to dissolve when the cars initially at the head of the jam are allowed to continue traveling. The car trajectory plots shows how they instantaneously pass into, and rapidly through the zone $(0, 1\,\text{mi})$ with increased maximum velocity, and abruptly slow down again when entering the section $x > 1\,\text{mi}$. In both cases, sharp discontinuities are formed at both ends of the high velocity zone. One detail is, however, differs between Example 1 and Example 2: in Example 1, the density decreases smoothly for $x < 0$. Due to the concave shape of the flux density function, the entropy condition excludes backwards propagating discontinuities with high density upstream and low density downstream. As a consequence, in the absence of x-dependent flux discontinuities, backward traveling waves are always rarefaction waves. The smooth variation of the density for $x < 0$ is also reflected in the car trajectory plot of Figure 3, showing that cars gradually accelerate from rest. In contrast to this, the solution for Example 2 in Figure 4 displays a backwards propagating shock denoting an abrupt decrease from $\rho_{\max}$ to the value $\rho^*_{\max} = 128.035\,\text{cars/mi}$, which has the property that the tangent to the graph of $v_{\max} f(\rho)$ in the point $(\rho^*_{\max}, f(\rho^*_{\max}))$ cuts the graph of that function in $\rho = \rho_{\max}$, see Figure 2. This indicates a backwards propagating contact discontinuity followed by a smooth variation of ρ. The car trajectories in Figure 4 indicate that under the assumptions of the non-convex model, cars instantaneously accelerate from rest to the velocity $v_{\max} f(\rho^*_{\max})/\rho^*_{\max}$, which produces a kink in the trajectories. This difference in behaviour is, of course, not related to the presence of an x-dependent flux discontinuity.

4.1.2. *A finite road segment with reduced maximum velocity (Example 3).* The more typical situation is that of Case A, i.e., we have an isolated road segment which enforces a reduction of the maximum velocity. These kinds of 'bottleneck' problems were already studied in the early paper by Lighthill and Whitham [24]. Moreover, in this and all subsequent examples we limit the discussion to the convex function $f(\rho) = f_{\mathrm{DG}}(\rho)$. Specifically in Example 3, which we simulate for later comparison with the corresponding case for the diffusively corrected Model 1, we choose $v^0_{\max} = 70\,\text{mph}$ and $v^*_{\max} = 25\,\text{mph}$. The initial density is chosen as

$$\rho_0(x) = \begin{cases} 100\,\text{cars/mi} & \text{for } -2\,\text{mi} \le x \le -1\,\text{mi}, \\ 0 & \text{otherwise.} \end{cases}$$

For example, we may imagine a convoy of cars traveling on an otherwise empty road, and wish to see how this convoy passes through the reduced speed road segment. The numerical solution to this problem has been calculated with $\Delta x = 1/200\,\text{mi}$ and $\lambda = 0.002\,\text{h/mi}$, and is displayed in Figures 5 and 6. We observe that this relatively simple setting produces a quite complicated solution structure. We observe that the convoy first dilutes, and that cars upon arriving at the speed reduction interface $x = 0$ form a concentrated traffic 'jam'. This jam is visible as a thin nearly triangular-shaped structure where the density assumes the constant value $\rho = 188.76\,\text{cars/mi}$. The tail of this traffic jam propagates backwards as a curved shock until the last cars from the initial convoy arrive. Since the cars from the traffic jam pass into the reduced speed zone, the tail of the jam recedes. After about 8 minutes, all cars have left the zone $x \le 0$, and after about 14 minutes, all cars have passed into the high-speed zone $x > 1\,\text{mi}$. Figure 6 shows that all cars (except the one initially located at $x = -1\,\text{mi}$) pass through three density continuities (the above-mentioned curved shock and the stationary shocks at $x = 0$ and $x = 1\,\text{mi}$) associated with abrupt speed changes.

4.1.3. *Heavy rain falling on a portion of the highway (Example 4).* We consider an application to a real problem introduced by Mochon [26] assuming that at time $t = 0$, heavy rain starts to fall on the highway segment $[a, b] = [0, 1]$. This rainfall causes vehicles to slow down on that segment and thus produces problem of Case A according to Section 2.2. To be specific, we assume the parameters $v^0_{\max} = 70\,\text{mph}$ and $v^*_{\max} = 35\,\text{mph}$. We now assume, however, that the rainfall is short and lasts only twelve minutes or $0.2\,\text{h}$, and that after that time the maximum speed is $v^0_{\max}$ again on the entire highway. Mochon [26] presents a complete solution of that problem by

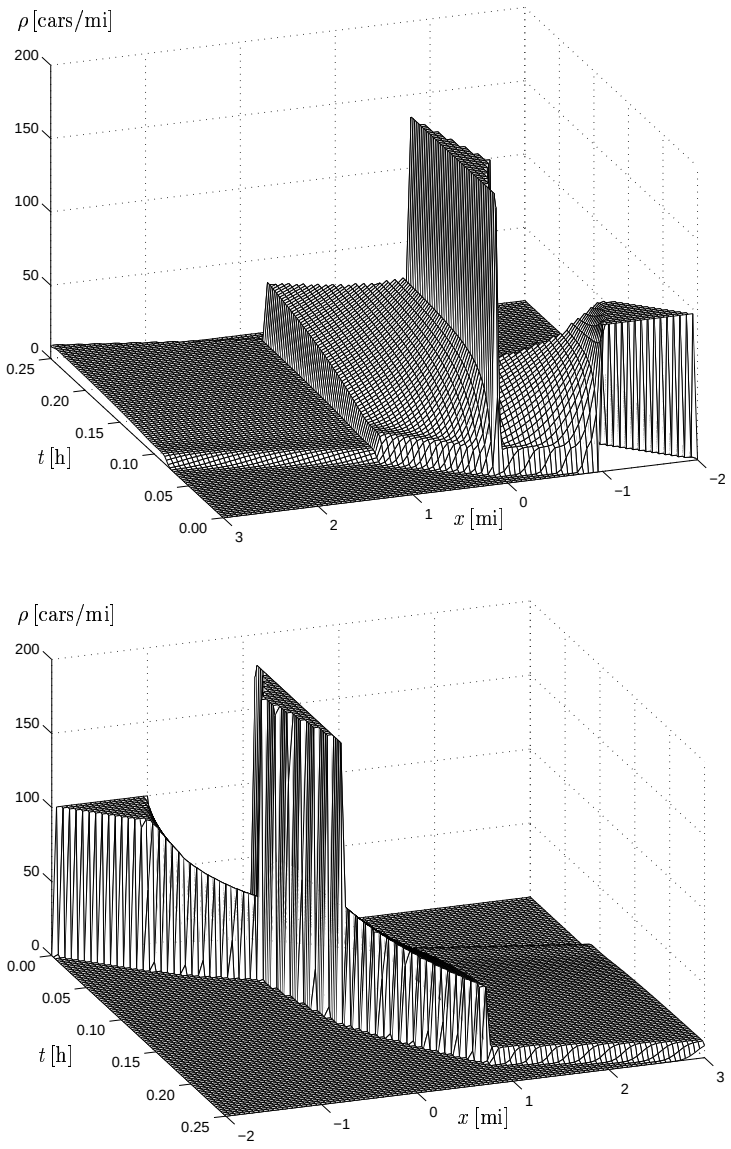

FIGURE 5. Example 3: A finite convoy of cars moving along a road with a finite segment of reduced maximum velocity ahead (Case A): two different aspects of the numerical solution calculated by using $f(\rho) = f_{\mathrm{DG}}(\rho)$.

the method of characteristics. We present a simulation of the same case using the convex flux function $f = f_{\mathrm{DG}}(\rho)$, the parameters $\lambda = 0.002\,\mathrm{h/mi}$ and $\Delta x = 1/100\,\mathrm{mi}$, and starting from an initial density $\rho_0 = 50\,\mathrm{cars/mi}$. In Section 4.2 the same case will be considered for the diffusively corrected model.

Figures 7 and 8 show the numerical solution of this problem. Figure 7 shows the density ρ as a function of x and t, while Figure 8 displays trajectories $x = x(t)$ of cars whose position at $t = 0$ is an integer number of miles. The solution calculated numerically agrees in every detail with Mochon's construction [26]. In particular, we observe a strong density discontinuity propagating backwards from $x = 0$ at constant speed as long as the rain persists. At $t = 0.2\,\mathrm{h}$, the rain stops. As explained in detail in [26], the situation normalized again by two rarefaction waves emerging from $(x, t) = (0, 0.2\,\mathrm{h})$ and $(1\,\mathrm{mi}, 0.2\,\mathrm{h})$, respectively. The rarefaction emerging from $(0, 0.2\,\mathrm{h})$

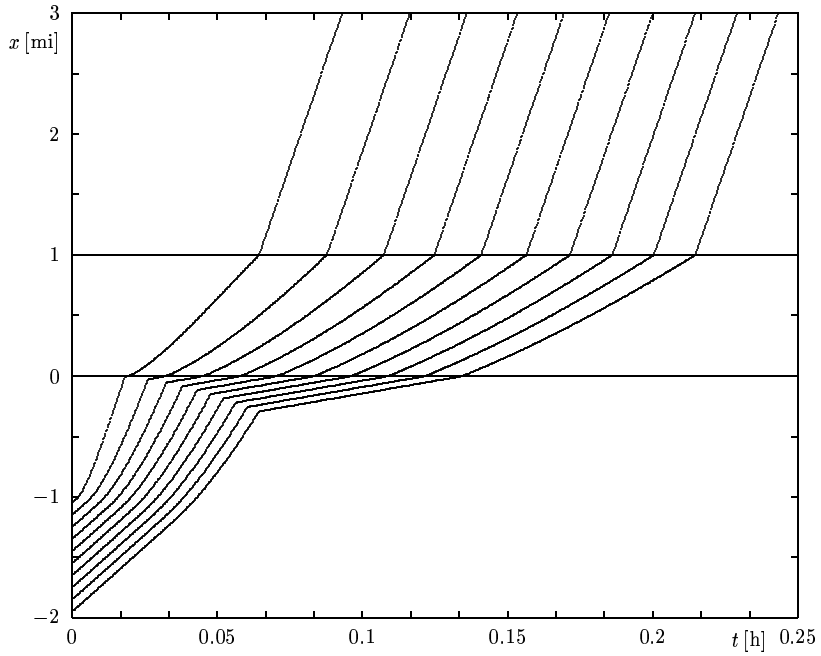

FIGURE 6. Example 3: A finite convoy of cars moving along a road with a finite segment of reduced maximum velocity ahead (Case A): trajectories (corresponding to the numerical solution of Figure 5) of cars starting from $x_i = -1.95 + i \cdot 0.1$ mi, $i = 0, \dots, 9$.

soon meets the strong shock mentioned above. By the intersection with the rarefaction, the shock becomes curved and decreases in strength. The trajectory of that shock can also be traced by the succession of kinks in the car trajectories in Figure 8 when cars enter the zone affected by the rainfall.

4.2. **Simulations of the diffusively corrected kinematic traffic model with changing road surface condition.** We first perform the calculations for the simpler Model 1. It is easy to check that the function $V(\rho) = V_{\mathrm{DG}}(\rho)$ given by (2.15) leads to

$$r\big(\rho, \tau; L(\rho)\big) = r_{\mathrm{DG}}\big(\rho, \tau; L(\rho)\big) = \begin{cases} 0 & \text{for } \rho \le \rho_{\mathrm{c}}, \\ CL(\rho) - C^2 \tau v_{\max} & \text{for } \rho > \rho_{\mathrm{c}}. \end{cases}$$

Moreover, we adopt here the following parameters given in [28]: $a = 0.1g$, where g is the acceleration of gravity, and $L_{\min} = 0.05$ mi. Consequently, we obtain from (2.16)

$$\begin{aligned} L(\rho) &= \max\left\{ \frac{(v^0_{\max})^2}{2a} C^2 \big(\ln(\rho_{\max}/\rho)\big)^2, L_{\min} \right\} \\ &= \begin{cases} L_0 \big(\ln(220/\rho)\big)^2 & \text{for } \rho < \rho^* := 78.219805 \,\text{cars/mi}, \\ 0.05 \,\text{mi} & \text{for } \rho > \rho^*, \end{cases} \qquad L_0 := 0.046756393 \,\text{mi}. \end{aligned} \tag{4.4}$$

We may now write the integrated diffusion coefficient for Model 1 as $D_1(\rho) = v^0_{\max} R_1(\rho)$, where

$$R_1(\rho) := \begin{cases} 0 & \text{for } \rho \le \rho_{\mathrm{c}}, \\ \mathcal{R}_{\mathrm{DG}}(\rho) - \mathcal{R}_{\mathrm{DG}}(\rho_{\mathrm{c}}) & \text{for } \rho > \rho_{\mathrm{c}}, \end{cases} \quad \mathcal{R}_{\mathrm{DG}}(\rho) := \int_0^\rho r_{\mathrm{DG}}\big(s, \tau; L(s)\big)\, ds. \tag{4.5}$$

Fix a lower bound of integration $\rho_0 < \rho_{\mathrm{c}}$. For $\rho_0 \le s \le \rho^*$, we obtain $\mathcal{R}_{\mathrm{DG}}(\rho) = \mathcal{R}^1_{\mathrm{DG}}(\rho)$ with

$$\mathcal{R}^1_{\mathrm{DG}}(\rho) = \int_{\rho_0}^{\rho} \big(CL(s) - C^2 \tau v_{\max}\big)\, ds$$

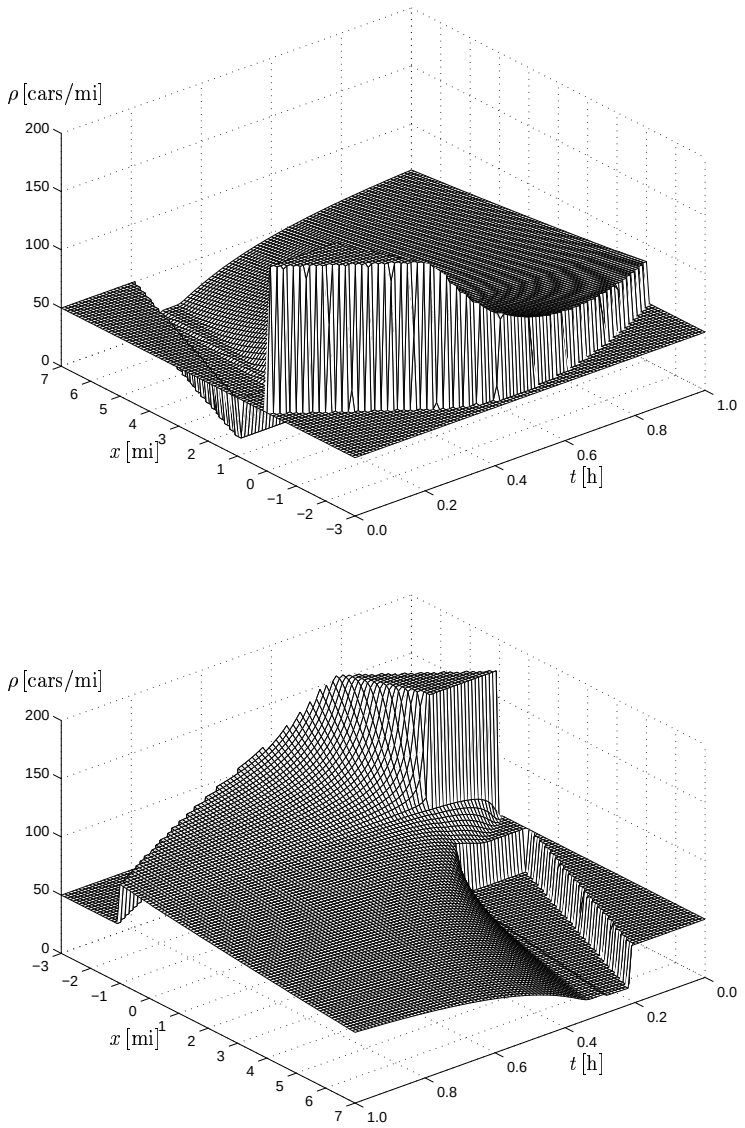

FIGURE 7. Example 4: The 'heavy rainfall problem' according to Mochon [26]: two different aspects of the numerical solution.

$$
\begin{aligned}
&= CL_0 \int_{\rho_0}^{\rho} \big(\ln(\rho_{\max}/s)\big)^2 \, ds - C^2 \tau v_{\max}^0 (\rho - \rho_0) \\
&= CL_0 \Big(\big((\ln \rho_{\max})^2 + 2 \ln \rho_{\max} + 2\big) s - 2(\ln \rho_{\max} + 1) s \ln s + s(\ln s)^2 \Big) \Big|_{s=\rho_0}^{\rho} \\
&\quad - C^2 \tau v_{\max}^0 (\rho - \rho_0).
\end{aligned}
$$

For $\rho > \rho^*$ we obtain

$$
\begin{aligned}
\mathcal{R}_{\mathrm{DG}}(\rho) &= \mathcal{R}_{\mathrm{DG}}^1(\rho^*) + \int_{\rho^*}^{\rho} \big(CL_{\min} - C^2 \tau v_{\max}^0\big) \, ds \\
&= \mathcal{R}_{\mathrm{DG}}^1(\rho^*) + \big(CL_{\min} - C^2 \tau v_{\max}^0\big)(\rho - \rho^*).
\end{aligned}
$$

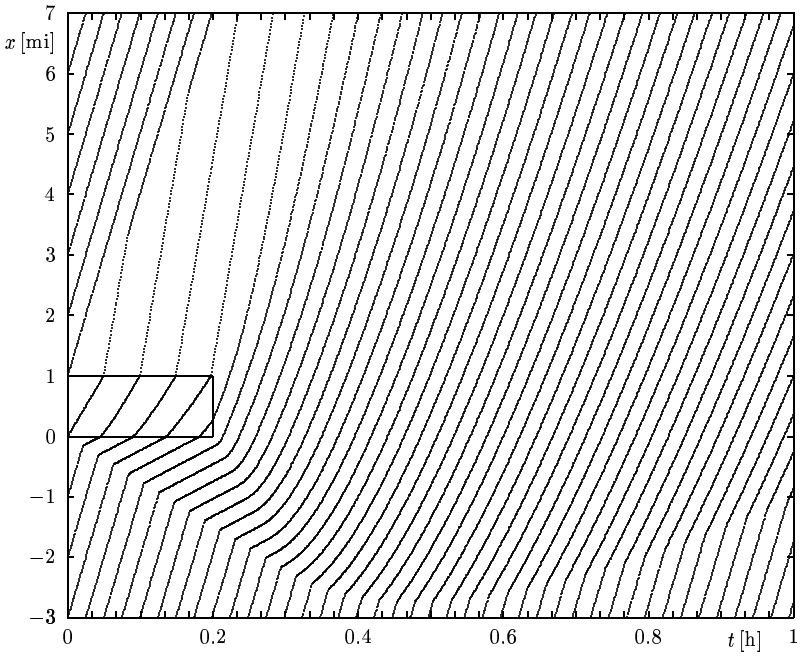

FIGURE 8. Example 4: The 'heavy rainfall problem' according to Mochon [26]: car trajectories of cars starting from $x_i(0) = i$, $i \in \mathbb{Z}$.

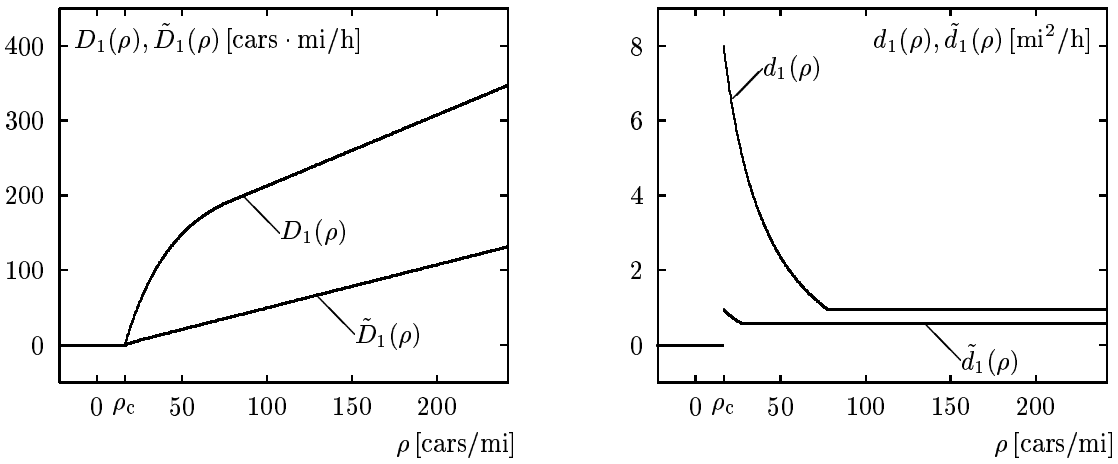

FIGURE 9. The integrated diffusion coefficients $D_1(\rho)$ and $\tilde{D}_1(\rho)$ (left) and their derivatives $d_1(\rho) = D_1'(\rho)$ and $\tilde{d}_1(\rho) = \tilde{D}_1'(\rho)$ (right).

Inserting $\tau = 2\,\mathrm{s} = 0.000\bar{5}\,\mathrm{h}$ and the numerical values of the other parameters ($C = \mathrm{e}/7$, $L_{\min} = 0.05\,\mathrm{mi}$, $v^0_{\max} = 70\,\mathrm{mph}$ and ρ^* and L_0 as given by (4.4)), we obtain $D_1(\rho)$, measured in cars$\cdot$mph, given by

(4.6)
$$D_1(\rho) = \begin{cases} 0 & \text{for } \rho \le \rho_{\mathrm{c}}, \\ 1.27099 \cdot \big(41.878\rho - 12.787\rho \ln \rho + \rho(\ln \rho)^2\big) - 0.4105\rho - 286.54 & \text{for } \rho_{\mathrm{c}} < \rho \le \rho^*, \\ 117.9003 + 0.94864\rho & \text{for } \rho > \rho^*. \end{cases}$$

We also provide one numerical example in which the predictions of Model 1 and Model 2 are compared. We consider Case A as before, and set $v^0_{\max} = 70\,\mathrm{mph}$ and $v^*_{\max} = v^0_{\max}/2 = 35\,\mathrm{mph}$.

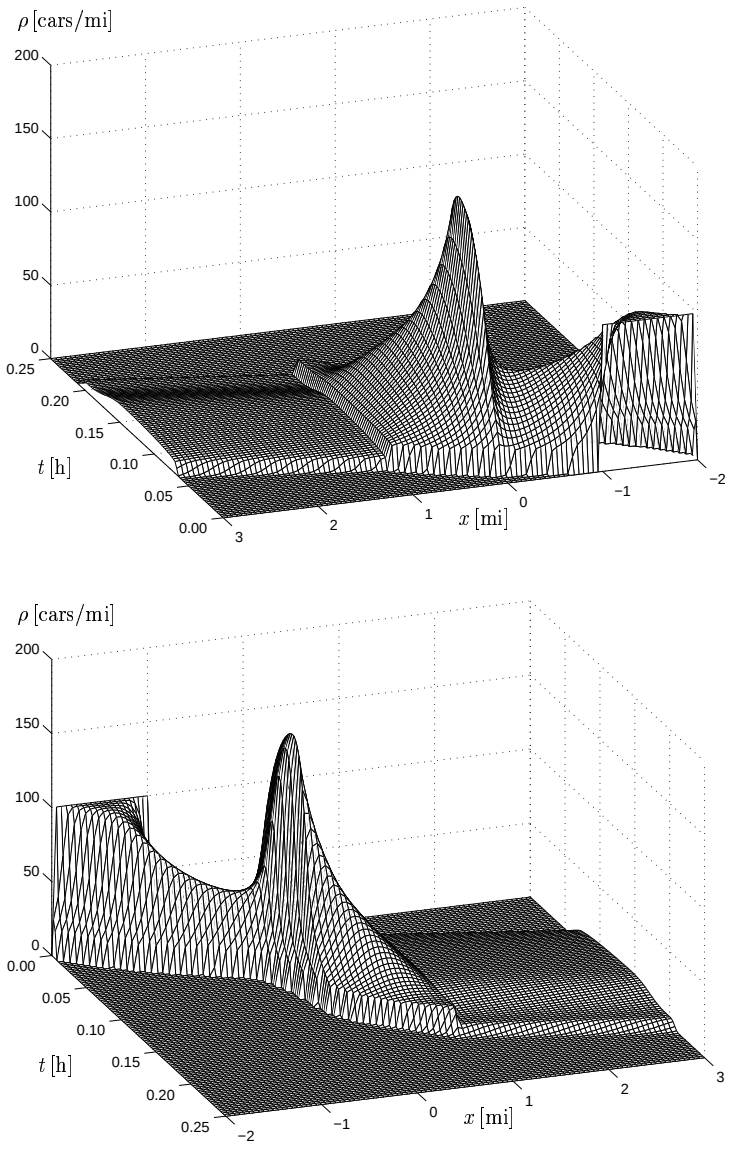

FIGURE 10. Example 5: A finite convoy of cars moving along a road with a finite segment of reduced maximum velocity ahead (Case A): two different aspects of the numerical solution for the diffusively corrected kinematic-wave model with uniform driver reaction (Model 1).

Since $v_{\max}(x)$ assumes just two different values, our governing equation is (2.17) with

$$D_2\big(\rho,\gamma(x)\big) = \begin{cases} D_1(\rho) & \text{if } \gamma(x) = v_{\max}(x) = 70\,\text{mph}, \\ \tilde{D}_1(\rho) & \text{if } \gamma(x) = v_{\max}(x) = 35\,\text{mph}, \end{cases} \tag{4.7}$$

where the diffusion function $\tilde{D}_1(\rho)$ is calculated in the same way as $D_1(\rho)$ but with $v^0_{\max}$ replaced by $v^0_{\max}/2$. Noting that the anticipation length function also has to be modified, i.e., we now use

$$\tilde{L}(\rho) = \max\left\{ \frac{(v^0_{\max})^2}{8a} C^2 \big(\ln(\rho_{\max}/\rho)\big)^2, L_{\min} \right\}$$

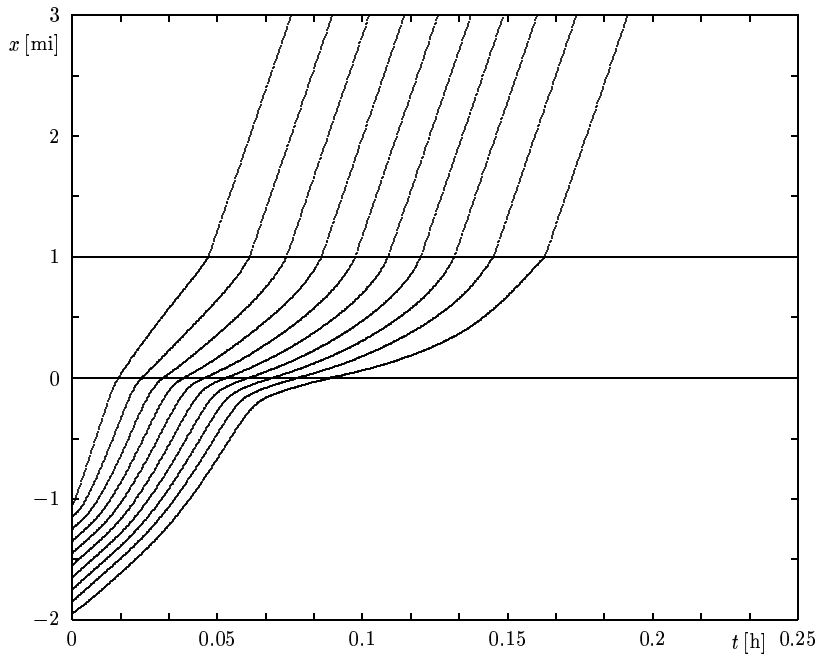

FIGURE 11. Example 5: A finite convoy of cars moving along a road with a finite segment of reduced maximum velocity ahead (Case A) for the the diffusively corrected kinematic-wave model: trajectories (corresponding to the numerical solution of Figure 10) of cars starting from $x_i = -1.95 + i \cdot 0.1\,\mathrm{mi}$, $i = 0, \dots, 9$.

$$= \begin{cases} \tilde{L}_0\big(\ln(220/\rho)\big)^2 & \text{for } \rho \le \tilde{\rho}^* := 27.810627\,\mathrm{cars/mi}, \\ 0.05\,\mathrm{mi} & \text{for } \rho > \tilde{\rho}^*, \end{cases} \qquad \tilde{L}_0 := 0.011689098\,\mathrm{mi}$$

instead of (4.4), we can easily derive the explicit formula (where $\tilde{D}_1(\rho)$ is given in cars $\cdot$ mph)

$$\tilde{D}_1(\rho) = \begin{cases} 0 & \text{for } \rho \le \rho_{\mathrm{c}}, \\ 0.15887\big(41.878\rho - 12.787\rho\ln\rho + \rho(\ln\rho)^2\big) - 0.10263\rho - 34.958 & \text{for } \rho_{\mathrm{c}} < \rho < \tilde{\rho}^*, \\ -7.8438 + 0.57694\rho & \text{for } \rho \ge \tilde{\rho}^*. \end{cases}$$

Figure 9 shows the integrated diffusion coefficients $D_1(\rho)$ and $\tilde{D}_1(\rho)$ and the diffusion functions $d_1(\rho) := D_1'(\rho)$ and $\tilde{d}_(\rho) = \tilde{D}_1'(\rho)$. Observe that both functions d_1 and $\tilde{d}_1$ are discontinuous at $\rho = \rho_{\mathrm{c}}$, and that our function $d_1(\rho)$ is the same as the diffusion coefficient plotted in Nelson's [28] Figure 2. Before proceeding with the discussion of numerical results, we recall that the singular mapping $\Psi(\gamma, \rho)$ (introduced in (3.11)) corresponding to the functions $f(\rho) = f_{\mathrm{DG}}(\rho)$ and $D_1(\rho)$ as given by (4.6) is plotted in Figure 1.

4.2.1. *A finite road segment with reduced maximum velocity (Example 5).* We select the situations of Examples 3 and 4 for comparison between the kinematic-wave model and Model 1 with driver reaction. The initial condition and parameters for Example 5 are the same as for Example 4, except that we use $\lambda = 0.0003\,\mathrm{h/mi}$. Figure 10 shows that this solution is more smoothed out than the solution of Figure 7. In particular, and in contrast to Figure 7, in Figure 10 the concentration varies continuously across the maximum velocity jump interface $x = 0$. The jam of cars formed by the abrupt maximum velocity reduction is less dense (i.e., leads to a lower peak) than in the kinematic-wave case. The car trajectories plotted in Figure 11 reveal that the velocities vary continuously, except across the interface at $x = 1\,\mathrm{mi}$, where for the last vehicles of the convoy, the local car density becomes so dilute that we fall back to the first-order hyperbolic equation. Another observation worth noting in this example is that the convoy passes more rapidly through the bottleneck under the diffusively corrected model; the first cars of the convoy need about one

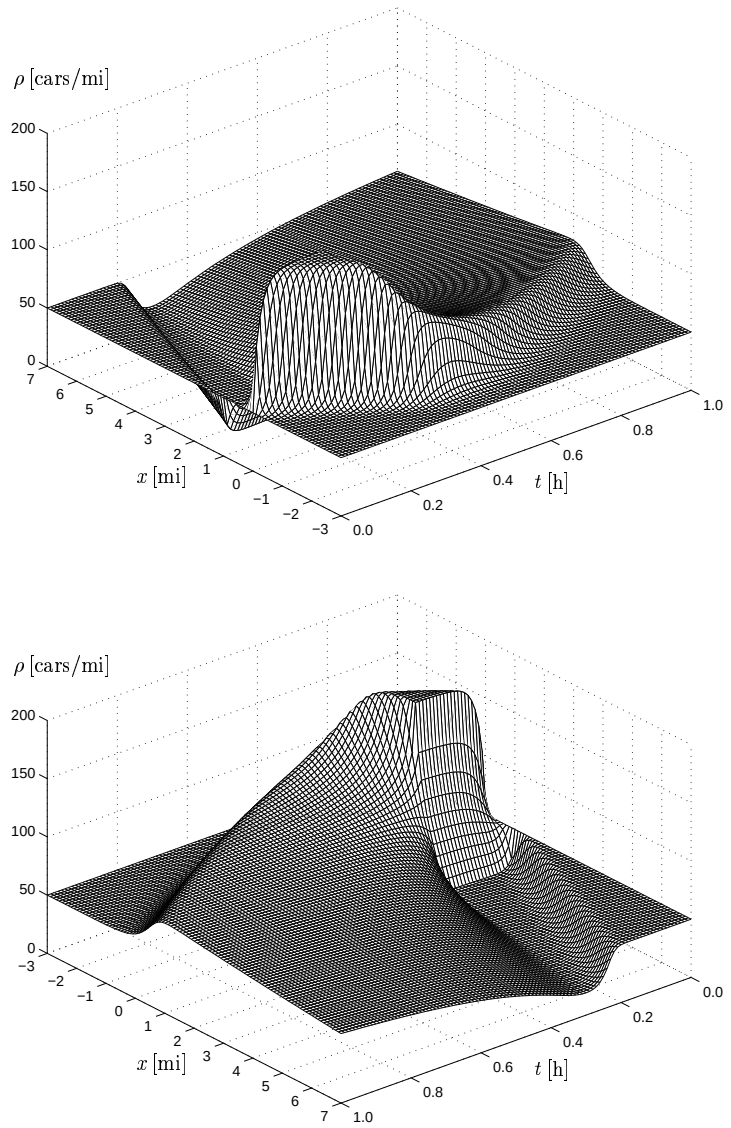

FIGURE 12. Example 6: The 'heavy rainfall problem' for the diffusively corrected kinematic-wave model with uniform driver reaction (Model 1): two different aspects of the numerical solution.

minute less time to travel from $x = -2\,\mathrm{mi}$ to $x = 3\,\mathrm{mi}$, while the last cars even save around three minutes. This may well illustrate the benefits of driving with anticipation. The degenerate character of the diffusion becomes apparent in the abrupt transitions from dense traffic regions to zero density, corresponding to a jump from ρ_c to zero.

4.2.2. *The 'heavy rainfall problem' solved by the diffusively corrected kinematic-wave model (Example 6).* In a similar fashion, we now recalculate the 'heavy rainfall' problem with the diffusively corrected Model 1. Comparing Figures 7 and 12, we again see that the diffusion term causes the solution to be smoothed out. In particular we observe that there are no discontinuities associated with $x = 0$ and $x = 1$, and all car trajectories plotted in Figure 13 are smooth. The diffusively corrected model predicts slightly slower travel times from $x = -3\,\mathrm{mi}$ to $x = 7\,\mathrm{mi}$, although the time saved in most cases is about one minute. It should also be mentioned that under the kinematic

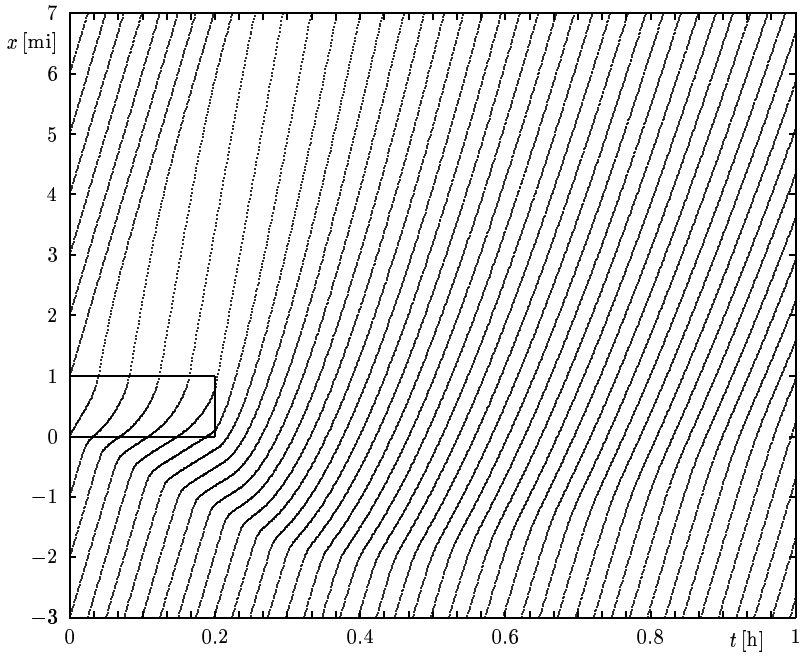

FIGURE 13. Example 6: The 'heavy rainfall problem' for the diffusively corrected kinematic-wave model with uniform driver reaction (Model 1): car trajectories of cars starting from $x_i(0) = i$, $i \in \mathbb{Z}$.

model the disturbed zone, marked by the curved shock, reaches further back (Figure 7 shows that the extreme position of the curved shock is about $x = -2.8$mi) than with the diffusively corrected one. A related observation is that at time $t = 1$h, the density of the diffusively corrected model has renormalized again roughly for $x \leq -0.7$mi, while at that same time, the curved shock of the kinematic model is still located near $x = -1.1$ mi.

4.2.3. *Comparison between Model 1 and Model 2 (Examples 7 and 8).* So far the numerical examples for the diffusively corrected models have been limited to Model 1, in part because for that model (and not yet for Model 2) a closed well-posedness theory is available. We now present a pair of numerical examples that demonstrate that the difference between the two models is significant. To this end, we consider again Case A and alternatively Model 1 and Model 2 with the data and diffusion coefficients given above, and drawn in Figure 9. Moreover, we assume the initial datum

$$\rho_0(x) = \begin{cases} 30\,\text{cars/mi} & \text{for } -4\,\text{mi} \leq x \leq 0, \\ 0 & \text{otherwise.} \end{cases}$$

Figures 14 and 15 show the numerical result for Model 1, corresponding to using the integrated diffusion coefficient $D_1(\rho)$ throughout, while Figures 16 and 17 correspond to Model 2, which employs (in this case) the integrated diffusion function $D_2(\rho, \gamma(x))$ defined by (4.7). We observe that the solutions differ significantly in the two cases. In particular, the maximum car density in the 'jam' forming near $x < 0$ is higher for Model 2 than for Model 1. This is remarkable in that the jam is formed before the cars enter the zone in which the two models are different.

ACKNOWLEDGMENTS

This work has been supported by the Collaborative Research Center (Sonderforschungsbereich) 404 at the University of Stuttgart, the BeMatA program of the Research Council of Norway, and the European network HYKE, funded by the EC as contract HPRN-CT-2002-00282.

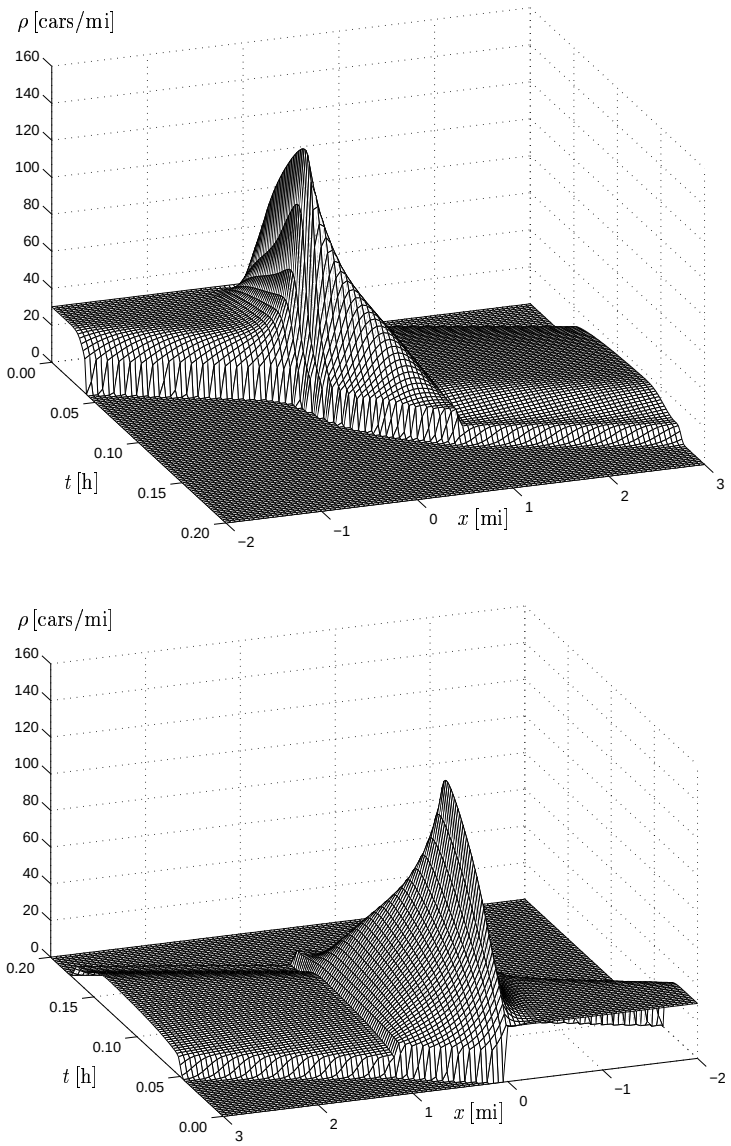

FIGURE 14. Example 7: Comparison between the diffusively corrected kinematic-wave Model 1 and Model 2: a finite convoy of cars moving along a road with a finite segment of reduced maximum velocity ahead (Case A): two different aspects of the numerical solution for the model with uniform driver reaction (Model 1).

REFERENCES

[1] A. Aw and M. Rascle, *Resurrection of "second order" models of traffic flow SIAM J. Appl. Math.* **60** (2000) 916–938.

[2] N. Bellomo, A. Marasco and A. Romano, *From the modelling of driver's behavior to hydrodynamic models and problems of traffic flow, Nonlin. Anal. Real World Appl.* **3** (2002) 339–363.

[3] I. Bonzani, *Hydrodynamic models of traffic flow: drivers' behaviour amd nonlinear diffusion, Math. Comp. Modelling* **31** (2000) 1–8.

[4] A. Bressan, *Hyperbolic Systems of Conservation Laws: The One-Dimensional Cauchy Problem* (Oxford Univeristy Press, 2000).

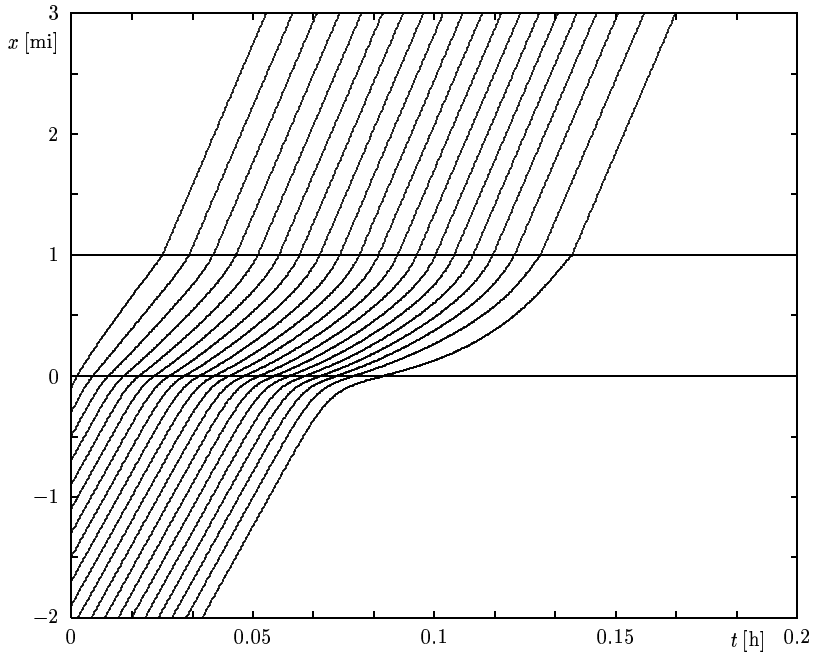

FIGURE 15. Example 7: Comparison between the diffusively corrected kinematic-wave Model 1 and Model 2: a finite convoy of cars moving along a road with a finite segment of reduced maximum velocity ahead (Case A): trajectories (corresponding to the numerical solution of Figure 14) of cars starting from $x_i = -3.9 + i \cdot 0.2\,\mathrm{mi}$, $i = 0, \ldots, 19$, corresponding to Model 1.

[5] R. Bürger and K.H. Karlsen, *A mathematical model of continuous sedimentation of flocculated suspensions in clarifier-thickener units.* In preparation.

[6] R. Bürger, K.H. Karlsen, C. Klingenberg and N.H. Risebro,*A front tracking approach to a model of continuous sedimentation in ideal clarifier-thickener units, Nonlin. Anal. Real World Appl.* **4** (2003) 457-481.

[7] R. Bürger, K.H. Karlsen, N.H. Risebro and J.D. Towers, *Well-posedness in BV_t and convergence of a difference scheme for continuous sedimentation in ideal clarifier-thickener units*, Preprint, available at the URL `http://www.math.ntnu.no/conservation/`, 2003.

[8] C.M. Dafermos, *Hyperbolic Conservation Laws in Continuum Physics* (Springer, 2000).

[9] C.F. Daganzo, *Requiem for second-order fluid approximations of traffic flow, Transp. Res. B* **29B** (1995) 277–286.

[10] A.C. Dick, *Speed/flow relationships within an urban area Traffic Eng. Control* **8** (1996) 393–396.

[11] B. Engquist and S. Osher, *One-sided difference approximations for nonlinear conservation laws, Math. Comp.***36** (1981) 321–351.

[12] D.C. Gazis (Ed.), *Traffic Science* (Wiley, 1974).

[13] H. Greenberg, *An analysis of traffic flow, Op. Res.* **7** (1979) 79–85.

[14] J.M. Greenberg, *Extensions and amplifications of a traffic model of Aw and Rascle, SIAM J. Appl. Math.* **62** (2001) 729–745.

[15] H. Holden and N.H. Risebro, *A mathematical model of traffic flow on a network of unidirectional roads, SIAM J. Math. Anal.* **26** (1995) 999–1017.

[16] H. Holden and N.H. Risebro,*Front Tracking for Conservation Laws* (Springer, 2002).

[17] W.L. Jin and H.M. Zhang, *The formation and structure of vehicle clusters in the Payne-Whitham traffic flow model, Transp. Res. B* **37** (2003) 207–223.

[18] K.H. Karlsen, N.H. Risebro and J.D. Towers, *Upwind difference approximations for degenerate parabolic convection-diffusion equations with a discontinuous coefficient, IMA J. Numer. Anal.* **22** (2002) 623–664.

[19] K.H. Karlsen, N.H. Risebro, and J.D. Towers, *On a nonlinear degenerate parabolic transport-diffusion equation with a discontinuous coefficient, Electron. J. Diff. Eqns.* **2002** (2002) 1-23.

[20] K.H. Karlsen, N.H. Risebro and J.D. Towers, *L^1 stability for entropy solutions of degenerate parabolic convection-diffusion equations with discontinuous coefficients*, Preprint, available at the URL `http://www.math.ntnu.no/conservation/`, 2003.

[21] T. Li, *Global solutions and zero relaxation limit for a traffic flow model, SIAM J. Appl. Math.* **61** (2001) 1042–1061.

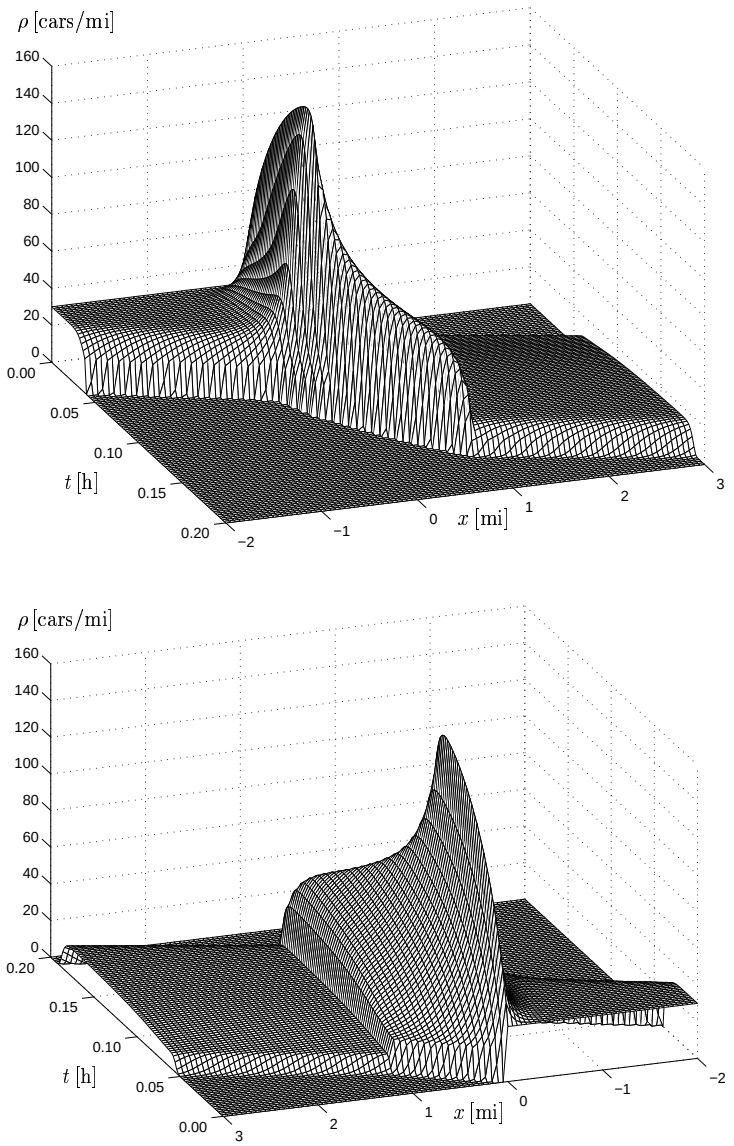

FIGURE 16. Example 8: Comparison between the diffusively corrected kinematic-wave Model 1 and Model 2: a finite convoy of cars moving along a road with a finite segment of reduced maximum velocity ahead (Case A): two different aspects of the numerical solution for the model with maximum-speed-adapted driver reaction (Model 2).

[22] T. Li, *Well-posedness theory of an inhomogeneous traffic flow model, Discr. Cont. Dyn. Syst. Ser. B* **2** (2002) 401–414.
[23] M.J. Lighthill and G.B. Whitham, *On kinematic waves. I. Flood movement in long rivers, Proc. Roy. Soc. London. Ser. A* **229** (1955) 281–316.
[24] M.J. Lighthill and G. B. Whitham, *On kinematic waves. II. A theory of traffic flow on long crowded roads, Proc. Roy. Soc. London. Ser. A* **229** (1955) 317–345.
[25] A.D. May, *Traffic Flow Fundamentals* (Prentice Hall, 1990).
[26] S. Mochon, *An analysis of the traffic on highways with changing surface conditions, Math. Modelling* **9** (1987) 1–11.

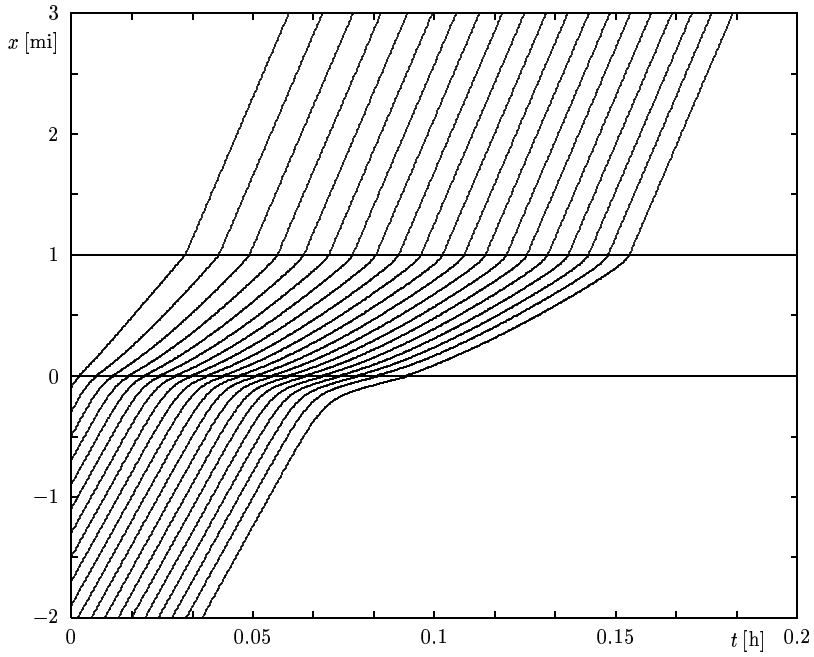

FIGURE 17. Example 8: Comparison between the diffusively corrected kinematic-wave Model 1 and Model 2: a finite convoy of cars moving along a road with a finite segment of reduced maximum velocity ahead (Case A): trajectories (corresponding to the numerical solution of Figure 16) of cars starting from $x_i = -3.9 + i \cdot 0.2\,\mathrm{mi}$, $i = 0, \ldots, 19$, corresponding to Model 2.

[27] P. Nelson, *Synchronized traffic flow from a modified Lighthill-Whitham model, Phys. Rev. E* **61** (2000) R6052–R6055.

[28] P. Nelson, *Traveling-wave solutions of the diffusively corrected kinematic-wave model, Math. Comp. Modelling* **35** (2002) 561–579.

[29] P.I. Richards, *Shock waves on the highway, Oper. Res.* **4** (1956) 42–51.

[30] E. Rouvre and G. Gagneux, *Solution forte entropique de lois scalaires hyperboliques-paraboliques dégénérées, C. R. Acad. Sci. Paris Sér. I* **329** (1999) 599–602.

[31] A.I. Vol'pert and S. I. Hudjaev, *Cauchy's problem for degenerate second order quasilinear parabolic equations, Math. USSR Sbornik* **7** (1969) 365–387.

[32] H.M. Zhang, *Driver memory, traffic viscosity and a viscous vehicular traffic flow model, Transp. Res. B* **37** (2003) 27–41.